1 **SARS-CoV-2 B.1.1.7 and B.1.351 variants of concern induce lethal disease in K18-hACE2**

2 **transgenic mice despite convalescent plasma therapy**

3 Alexander M. Horspool[1,2], Chengjin Ye[9], Ting Y. Wong[1,2], Brynnan P. Russ[1,2], Katherine S. Lee[1,2],

4 Michael T. Winters[3], Justin R. Bevere[1,2], Theodore Kieffer[4], Ivan Martinez[4], Julien Sourimant[5],

5 Alexander Greninger[6], Richard K. Plemper[5], James Denvir[7], Holly A. Cyphert[8], Jordi Torrelles[9],

6 Luis Martinez-Sobrido[9], F. Heath Damron[1,2]*.

7

8 [1] Department of Microbiology, Immunology, and Cell Biology, West Virginia University,

9 Morgantown, WV, USA

10 [2] Vaccine Development Center at West Virginia University Health Sciences Center, Morgantown,

11 WV, USA

12 [3] West Virginia University Cancer Institute, Morgantown, WV, USA

13 [4] Department of Pathology, Anatomy and Laboratory Medicine, West Virginia University School

14 of Medicine, Morgantown, WV, USA

15 [5] Institute for Biomedical Sciences, Georgia State University, Atlanta, GA, USA

16 [6] University of Washington, Department of Laboratory Medicine and Pathology, Seattle,

17 Washington

18 [7] Department of Biomedical Sciences, Marshall University, Huntington, WV. USA

19 [8] Department of Biological Sciences, Marshall University, Huntington, WV, USA

20 [9] Texas Biomedical Research Institute, San Antonio, TX, USA.

21

22 * Corresponding author

23 Corresponding author email address: fdamron@hsc.wvu.edu

24 Lead contact email address: fdamron@hsc.wvu.edu

25

28 **SUMMARY:** SARS-CoV-2 variants of concern (VoCs) are impacting responses to the COVID-19

29 pandemic. Here we present a comparison of the SARS-CoV-2 USA-WA1/2020 (WA-1) strain with

30 B.1.1.7 and B.1.351 VoCs and identify significant differences in viral propagation *in vitro* and

31 pathogenicity *in vivo* using K18-hACE2 transgenic mice. Passive immunization with plasma from

32 an early pandemic SARS-CoV-2 patient resulted in significant differences in the outcome of VoC-

33 infected mice. WA-1-infected mice were protected by plasma, B.1.1.7-infected mice were partially

34 protected, and B.1.351-infected mice were not protected. Serological correlates of disease were

35 different between VoC-infected mice, with B.1.351 triggering significantly altered cytokine profiles

36 than other strains. In this study, we defined infectivity and immune responses triggered by VoCs

37 and observed that early 2020 SARS-CoV-2 human immune plasma was insufficient to protect

38 against challenge with B.1.1.7 and B.1.351 in the mouse model.

39

40

41 **INTRODUCTION:** The evolution of Severe Acute Respiratory Syndrome CoV-2 (SARS-CoV-2)

42 VoCs has been a source of escalating epidemiological alarm in the currently ongoing coronavirus

43 disease 2019 (COVID-19) pandemic. Mutants of SARS-CoV-2 have emerged and are thought to

44 be more infectious and more lethal than the early 2020 original Wuhan-Hu-1 or USA-WA1/2020

45 (WA-1) strains (Challen et al., 2021; Korber et al., 2020; Toyoshima et al., 2020). The VoC B.1.1.7,

46 first identified in the United Kingdom (Rambaut et al., 2020), and B.1.351, first identified in South

47 Africa (Tegally et al., 2020), are two emerging SARS-CoV-2 VoCs that are rapidly spreading

48 around the world and exhibit high levels of infectivity and therapeutic resistance (Challen et al.,

49 2021; Chen et al., 2021; Davies et al., 2021; Galloway et al., 2021; 2021b, 2021a; Wang et al.,

50 2021). Both VoCs harbor significant evolution in the receptor binding domain (RBD) of the spike

51 (S) viral glycoprotein (Rambaut et al., 2020; Tegally et al., 2020) that are predicted to impact

52 binding to the human angiotensin converting enzyme 2 (hACE2) viral receptor and enhance viral

53 entry to host cells (Bozdaganyan et al., 2021; Laffeber et al., 2021; Ozono et al., 2021; Shah et

54   al., 2020; Tian et al., 2021). In particular, B.1.1.7 contains the D614G, and N501Y, mutations in

55   the SARS-CoV-2 S RBD which are theorized to increase the ability of the virus to bind to hACE2

56   (Ozono et al., 2021; Tian et al., 2021). B.1.351 possesses these key mutations in the S RBD, in

57   addition to the K417N mutation E484K mutation which are not directly implicated in altered viral

58   transmission and hACE2 binding (Laffeber et al., 2021; Zhou et al., 2021). The culmination of

59   high infectivity, therapeutic resistance, and key changes in the viral genome suggests that these

60   VoCs may have an impact on pathogenicity in animal models of SARS-CoV-2. This could have

61   an impact on evaluating SARS-CoV-2 pathogenesis as well as prophylactic (vaccines) and

62   therapeutics (antivirals).

63   The K18-hACE2 transgenic mouse model (McCray et al., 2007) of SARS-CoV-2 infection

64   was established by Perlman and McCray among others in 2020 (Moreau et al., 2020; Oladunni

65   et al., 2020; Winkler et al., 2020). K18-hACE2 transgenic mice infected with SARS-CoV-2 exhibit

66   significant morbidity and mortality, viral tropism of the respiratory and central nervous systems,

67   elevated systemic chemokine and cytokine levels, significant tissue pathologies, and altered

68   gross clinical measures (Oladunni et al., 2020; Winkler et al., 2020; Yinda et al., 2021; Zheng et

69   al., 2021). The generation of this mouse model has led to numerous studies of SARS-CoV-2

70   infection for a variety of purposes including understanding SARS-CoV-2 related immunity, and

71   therapeutic / vaccine testing (Hassan et al., 2020; Kumari et al., 2020; Liu et al., 2021; Moreau et

72   al., 2020; Pandey et al., 2020; Sarkar and Guha, 2020; Silvas et al., 2021). As the world

73   experiences an increase in the number of SARS-CoV-2 VoCs, it is imperative to adapt existing

74   preclinical animal infection models to these newly emerging VoC. Specifically, it is critical to

75   understand if the K18-hACE2 transgenic mouse model first, is useful for studying SARS-CoV-2

76   VoC infection dynamics and second, if it exhibits any differences after challenge with newly

77   emerged SARS-CoV-2 VoCs. An investigation of these key points will provide context for studies

78   important for developing new therapeutics and prophylactics as the COVID-19 pandemic

79   continues and as new VoCs emerge.

80   Clinical studies of therapeutics and vaccines for COVID-19 have been complicated by the

81   rise of SARS-CoV-2 VoCs. Therapeutic escape by these mutants is documented (Wang et al.,

82   2021) and requires the development of novel treatment options as well as re-evaluation of existing

83   ones. One of the first treatment options for COVID-19 was infusion of convalescent plasma (CP).

84   CP exhibited some beneficial effects early in the pandemic for critically ill patients (Bloch, 2020;

85   Bloch et al., 2020; Chen et al., 2020), but its utility has recently been called into question

86   (Casadevall et al., 2021; Cele et al., 2021; NIH, 2021; Zhao and He, 2020). There are speculations

87   as to the reasons behind this, including that neutralizing antibodies (nAbs) generated against the

88   original Wuhan-Hu-1 or WA-1 SARS-CoV-2 S RBD may have different affinity to the new VoCs.

89   As many therapeutics and vaccines have focused on the RBD or S protein of SARS-CoV-2 Wuhan

90   or WA-1, it was of interest to determine whether early pandemic convalescent plasma containing

91   neutralizing antibodies against WA-1 SARS-CoV-2 S RBD protects against these VoCs with

92   mutations in their RBD. Thus, the overall focus of this study was to observe the effects of SARS-

93   CoV-2 VoCs on the K18-hACE2 transgenic mouse model of COVID-19, and determine whether

94   theses VoCs can evade an early COVID-19 pandemic therapeutic: CP treatment.

95

96   **METHODS:**

97   _Ethics and biosafety:_ Human plasma used in this study was obtained under WVU IRB no.

98   2004976401. Experiments with live SARS-CoV-2 virus were conducted in Biosafety Level 3 (BSL-

99   3) Texas Biomedical Research Institute (TBRI IBC BSC20-004) or West Virginia University (WVU

100   IBC 20-09-03).   All ABSL-3 animal experiments were conducted under West Virginia University

101   (WVU) ACUC protocol no. 2009036460.

102

103   _Viral growth and in vitro analysis of SARS-CoV-2 replication:_ SARS-CoV-2 USA-WA-1/2020 (NR-

104   52281) (WA-1), B.1.1.7 (NR-54000), and B.1.351 (NR-54008) strains were obtained from BEI

105   Resources and propagated in Vero E6 cells (ATCC-CRL-1586) as previously described (Case et

106   al., 2020; Oladunni et al., 2020). Vero E6 cells for viral titrations (6-well plate, 10^6 cells/well) were

107   infected with serial dilutions of SARS-CoV-2 WA-1, B.1.1.7 or B.1.351 VoCs. At 72 hours post-

108   infection, cells were fixed overnight with 10% formalin (Sigma HT501128-4L), permeabilized and

109   immunostained with 1µg/mL of a SARS-CoV cross-reactive nucleocapsid (N) protein antibody

110   1C7C7, kindly provided by Dr. Thomas Moran at the Icahn School of Medicine at Mount Sinai.

111   For viral growth kinetics, Vero E6 cells (6-well plate, 10^6 cells/well, triplicates) were infected (MOI

112   0.01) with SARS-CoV-2 WA-1, B.1.1.7 or B.1.351. At the indicated times after infection (12, 24,

113   48 and 72 hours), tissue culture samples were collected and titrated by plaque assay as described

114   previously (Oladunni et al., 2020).

115

116   _Sequencing of SARS-CoV-2 VoCs:_ SARS-CoV-2 viral RNA from all stocks used for _in vitro_

117   analyses was deep sequenced according to the method described previously (Ye et al., 2020a).

118   Briefly, we generated libraries using KAPA RNA HyperPrep Kit (Roche KK8541) with a 45 min

119   adapter ligation incubation including 6-cycle of PCR with 100 ng RNA and 7 mM adapter

120   concentration. Samples were sequenced on an Illumina Hiseq X machine. Raw reads were quality

121   filtered using Trimmomatic v0.39 (Bolger et al., 2014) and mapped to a SARS-CoV-2 reference

122   genome (Genbank Accession No. MN985325) with Bowtie2 v2.4.1 (Langmead and Salzberg,

123   2012). Genome coverage was quantified with MosDepth. version 0.2.6 (Pedersen and Quinlan,

124   2018). We genotyped each sample for low frequency VoCs with LoFreq* v2.1.3.1 (Wilm et al.,

125   2012) and filtered sites with allele frequencies less than 20%. SARS-CoV-2 viral RNA from stocks

126   used for K18-hACE2 transgenic mice infection was deep sequenced and reads were aligned to

127   the MN908947.3 reference genome using BWA version 0.7.17 (Li and Durbin, 2009) and trimmed

128   for base-calling quality using iVar version 1.3.1 (Grubaugh et al., 2019) with default parameters.

129   Consensus sequence and individual mutations relative to the reference genome were determined

130   using iVar, with a minimum allele frequency of 30% used as a threshold for calling a mutation.

131   Coverage was computed using samtools mpileup version 1.11 (Li et al., 2009). Lineage was

132 confirmed using pangolin version 2.3.5 and pangoLEARN version 2021-03-16 (O'Toole et al.).

133 Authentication of the B.1.351 stock was performed using metagenomic sequencing as described

134 previously (Addetia et al., 2020; Greninger et al., 2017). Viral RNA was treated with Turbo DNase

135 I (Thermo Fisher). cDNA was generated from random hexamers using SuperScript III reverse

136 transcriptase, second strand was generated using Sequenase 2.0, and cleaned using $0.8\times$

137 Ampure XP beads purification on a SciClone IQ (Perkin Elmer). Sequencing libraries were

138 generated using two-fifths volumes of Nextera XT on ds-cDNA with 18 cycles of PCR

139 amplification. Libraries were cleaned using $0.8\times$Ampure XP beads and pooled equimolarly before

140 sequencing on an Illumina NovaSeq (1×100bp run). Raw fastq reads were trimmed using

141 cutadapt (-q 20) (Martin). To interrogate potential resistance alleles, reference-based mapping to

142 NC_045512.2 was carried out using our modified Longitudinal Analysis of Viral Alleles (LAVA -

143 https://github.com/michellejlin/lava) (Jin et al., 2019) pipeline. LAVA constructs a candidate

144 reference genome from early passage virus using bwa (Li and Durbin, 2009), removes PCR

145 duplicates with Picard, calls variants with VarScan (Koboldt et al., 2009, 2012), and converts

146 these changes into amino acid changes with Annovar (Wang et al., 2010). The genome sequence

147 for strain B.1.351 is accession number MZ065365 and SRA BioProject PRJNA726258.

148

149

150 *Infection of K18-hACE2 transgenic mice with SARS-CoV-2 VoCs and treatment with human*

151 *plasma:* SARS-CoV-2 VoCs were thawed from -80ºC and diluted in infection medium (Dulbecco's

152 Modified Eagle Medium 4/.5g/L glucose + 2% fetal bovine serum + 1% HEPES + 1%

153 penicillin/streptomycin at 10,000 units/µg/mL) to a concentration of 10^6 plaque forming units (pfu)

154 /mL in the WVU BSL-3 high-containment facility. Male and female (Figures 2-3) or male (Figures

155 4-7) eight-week-old B6.Cg-Tg(K18-hACE2)2Prlmn/J mice (Jackson Laboratory 034860) were

156 anesthetized with a single intraperitoneal dose of ketamine (Patterson Veterinary 07-803-6637,

157   80 mg/kg) + xylazine (Patterson Veterinary 07-808-1947, 8.3 mg/kg) and the 50µL infectious dose

158   was administered with a pipette intranasally, 25µL per nare. 500µL of convalescent plasma (CP)

159   or healthy human sera (HHS) with known anti-SARS-CoV-2 IgGs and nAbs (Supplementary

160   Figure 1) were administered intraperitoneally at this time. Convalescent human plasma was

161   obtained from a single individual with PCR-confirmed SARS-CoV-2 infection in March 2020 via

162   WVU IRB no. 2004976401. Mice were monitored until awake and alert.

163

164   *Clinical scoring of SARS-CoV-2 infected mice:* Mice were scored daily on a scale encompassing

165   appearance (score of 0-2), eye health (score of 0-2), respiration (score of 0-2), activity (score of

166   0-3), weight loss (score of 0-5), and hypothermia (0-2) (Supplementary Figure 1). Appearance

167   included visual identification of a combination of mild to severe piloerection (0-2) or lack of

168   grooming (0-2). Eye health scores were defined by observation of squinting (1), prolonged eye

169   closure not related to sleep (2), or eye discharge (0-2) depending on severity. The maximal

170   combined score for eye health was 2. Respiration (assessed visually) outside the range of 80-

171   240 breaths per minute required mandatory euthanasia and scored as 2. Respiration that was

172   abnormal in regularity was scored as 1. Activity was scored as slow (1), immobile (2), or collapsed

173   and immobile (3). Weight loss was scored as 0-5% (0), 5-10% (1), 10-15% (2) 15-20% (3), >20%

174   (4-5). All mice with weight loss greater than 20% were humanely euthanized. Hypothermia was

175   assessed and scored as not-present (>36.4°C, 0), developing (36.4°C – 35.0°C, 1) or present

176   (<35.0°C, 2) (Supplementary Figure 1).

177

178   *Euthanasia and necropsy of SARS-CoV-2 infected mice:* Euthanasia was conducted by

179   administering 200 µL of pentobarbital (Patterson Veterinary 07-805-9296, 390 mg/kg diluted in

180   0.9% sterile NaCl) and cardiac puncture. Blood was aliquoted into gold serum separator tubes

181   (BD 365967) and centrifugated at 15,000 x *g* for 5 min. Serum was removed and stored in 1.5 mL

182   tubes at -80°C until needed. Lungs were removed from animals and the right lobes of the lung

183   were homogenized in 1mL of PBS in Miltentyi C tubes (Miltenyi Biotec 130-096-334) using the

184   m_lung_02 program on a Miltenyi gentleMACS tissue dissociator. An aliquot of each lung

185   homogenate (300µL) was added to 100µL of TRIReagent (Zymo Research R2050-1-200) and

186   stored at -80°C. Remaining homogenates (300µL) were spun down at 15,000 x g and the

187   supernatants collected. Pellets were frozen at -80°C until use. Brain tissue was removed from

188   animals and split down the mid-line. The right brain was added to 1mL of PBS in Miltenyi C tubes

189   and homogenized using the m_lung_02 program. An aliquot of each homogenate (500µL) was

190   added 167µL aliquots of TRIReagent and stored at -80°C until use. Remaining homogenates were

191   frozen at -80°C until use. To inactivate virus from tissue samples, 1% v/v Triton X-100 (Sigma-

192   Aldrich T8787) (Winkler et al., 2020) was added to each sample and incubated for 1 hour at room

193   temperature. Inactivated samples were then removed from the ABSL-3 facility.

194

195   *Evaluating viral copy number in SARS-CoV-2 infected tissues:* RNA from homogenized virus-

196   inactivated lung and brain tissues of SARS-CoV-2 infected animals was extracted using the

197   Direct-zol RNA MiniPrep Kit (Zymo Research R2051) following the manufacturer's instructions.

198   RT-PCR and qPCR were performed by generating a master mix of: 10µL of TaqMan RT-PCR Mix

199   from the Applied Biosystems TaqMan RNA to CT One Step Kit (Thermo-Fisher Scientific

200   4392938), 900nM (1.8µL) of (ATGCTGCAATCGTGCTACAA) forward nucleocapsid primer

201   (Winkler et al., 2020), 900nM (1.8µL) of (GACTGCCGCCTCTGCTC) reverse nucleocapsid primer

202   (Winkler   et   al.,   2020),   250nM   (0.5µL)   of   TaqMan   probe   (56-

203   FAM/TCAAGGAAC/ZEN/AACATTGCCAA/3IABkFQ), 0.5µL of TaqMan RT enzyme from the

204   Applied Biosystems TaqMan RNA to CT One Step Kit (Thermo-Fisher Scientific 4392938), 100ng

205   of RNA, and RNAse/DNAse free water to make a 20µL total reaction volume. Samples were run

206   in triplicate in Microamp Optical 96-well Fast Reaction Plates (Thermo-Fisher Scientific 4306737)

207   through the following protocol: reverse transcription at 48°C for 15 minutes, activation of AmpliTaq

208   Gold DNA polymerase at 95°C for 10 minutes, and 50 cycles of 95°C denaturing for 10 seconds

209 followed by 60°C annealing for 60 seconds. Samples were run on an Applied Biosystems

210 StepOnePlus Real-Time PCR System. Samples with undetectable virus were assigned a value

211 of 1. C_T values and copy numbers were calculated and analyzed in Microsoft Excel and GraphPad

212 Prism v9.0.0.

213

214 *Assessment of human IgGs against WA-1 SARS-CoV-2 S RBD and N:* Human IgGs against WA-

215 1 SARS-CoV-2 S RBD and N were quantified using ELISA as described previously (Horspool et

216 al., 2021). Briefly, WA-1 S RBD (2µg/mL) or N (1µg/mL) proteins were coated on plates and

217 blocked with 3% milk in 0.1% Tween 20 +PBS (PBS-T). Plates were washed three times with

218 PBS-T (200µL) and virus inactivated samples (25µL) from infected mice were added to 100µL of

219 sample buffer (1% milk + 0.1% Tween 20 diluted in PBS) and serially diluted (5-fold) down the

220 plates. The final row was left with 100µL of sample buffer as a negative control. Plates were

221 incubated for 10 minutes at room temperature shaking at 60rpm and subsequently washed four

222 times with PBS-T (200µL). Secondary antibody (100µL 1:500 anti-human IgG HRP, Invitrogen

223 31410) was added and plates were incubated for 10 minutes at room temperature shaking at

224 60rpm. After incubation, plates were washed five times with PBS-T (200µL) and SigmaFAST OPD

225 (Sigma-Aldrich P9187, 100µL) was added to each well of the plate. OPD development was

226 stopped with 25µL of 3M hydrochloric acid and plates were read at an absorbance of 492nm on

227 a Synergy H1 plate-reader. Area under the curve analysis was completed in GraphPad Prism.

228 Human samples used as a comparison in Supplementary Figure 4 were obtained via WVU IRB

229 no. 2004976401 as described previously (Horspool et al., 2021).

230

231 *Quantification of nAbs against WA-1 SARS-CoV-2 S RBD:* An assay to assess nAb levels was

232 developed using Luminex bead and Magpix technologies. SARS-CoV-2 S RBD (1µg) produced

233 at WVU as described previously(Horspool et al., 2021) was conjugated to Luminex MagPlex®

234 Microspheres (MC10012-YY) using the Luminex xMAP antibody coupling kit (Luminex 40-50016)

235   per the manufacturer's instructions. Conjugated beads (50µL containing 2000 beads suspended

236   in 1x PBS-TBN (Phosphate buffered saline + 0.1% bovine serum albumin + 0.02% Tween 20

237   +0.05% sodium azide) diluted in de-ionized water from 5x PBS-TBN (Teknova P0211) were

238   loaded into black non-binding Greiner 96-well plates (Greiner 655900). Human plasma/serum

239   samples (25µL) were added into 100µL of PBS in the first row of a second black non-binding

240   plate. Samples were serially diluted (5-fold dilution in PBS) down the plate. The final row contained

241   PBS as a negative control. Diluted serum samples (50µL) were added to the 96-well plate

242   containing the beads, creating a total reaction volume of 50µL beads (2000 beads), and 50µL

243   diluted serum. The plates were covered with foil and shaken at 700rpm for 1 hour at room

244   temperature. After shaking, beads were pelleted on a 96-well plate magnet and washed two times

245   for 2 minutes with 200µL of 1x PBS-TBN. Beads were pelleted on the magnet and the wash

246   solution removed. ACE2-biotin (100µL at 0.25µg/mL, Sino Biological Inc #: 10108-H08H-B) was

247   added to each well. Plates were covered with foil and shaken at 700rpm for 1 hour at room

248   temperature. After shaking, beads were pelleted on a 96-well plate magnet and washed two times

249   for 2 minutes with 200µL of 1x PBS-TBN. Beads were pelleted on the magnet and the wash

250   solution removed. Streptavidin-phycoerythrin (MOSS INC: SAPE-001) (100µL at 4µg/mL) was

251   added to each well. Plates were covered with foil and shaken at 700rpm for 30 minutes at room

252   temperature. After shaking, beads were pelleted on a 96-well plate magnet and washed two times

253   for 2 minutes with 200µL of 1x PBS-TBN. Beads were resuspended in 100µL of 1x PBS-TBN and

254   analyzed on a Luminex MagPix. Median fluorescent intensity values were plotted against serum

255   dilution factor, and a sigmoidal regression line was fitted to the data using GraphPad Prism v9.0.0.

256   Calculated half maximal inhibitory concentration (IC_{50}) values of the sigmoidal curves were plotted

257   separately as a measure of neutralizing capacity.

258

259   *Cytokine analysis of serum-treated SARS-CoV-2 VoC infected mice:* Virus-inactivated serum

260   samples or lung supernatants from SARS-CoV-2 VoC infected mice were added to a custom 8-

261 plex Mouse Magnetic Luminex Assay (R&D Systems LXSAMSM-08) including IL-6, TNF, IFN-γ,

262 IL-10, IL-27, IL-1β, IL-2, IL-13, and IL-17 at the recommended dilution factor (2-fold dilution).

263 Cytokine arrays were read on a Luminex MagPix instrument.

264

265 *Flow cytometry of SARS-CoV-2 infected K18-hACE2 transgenic mouse lungs:* Lung

266 homogenates were thawed and pelleted at 1000 x g for 5 minutes at 4°C. PharmLyse (BD

267 Biosciences 555899, 1mL of 1X solution) was added to each sample and homogenates were

268 incubated for 2 minutes at 37°C. Samples were then pelleted at 1000 x g for 5 minutes at 4°C.

269 Pellets were resuspended in 300μL of PBS + 1% v/v FBS and 150μL were added to 2μL of Mouse

270 BD F_c Block (BD Biosciences 553142). Homogenates in F_c block were incubated for 15 minutes

271 at 4°C. After blocking, 100μL were transferred into 2μL of antibody cocktail including 0.5μg of:

272 hamster anti-mouse CD3e BV510: BD Biosciences 563024, rat anti-mouse APC-Cy7: BD

273 Biosciences 552051, rat anti-mouse CD11b BB515: BD Biosciences 564454, rat anti-mouse

274 CD8a BD Biosciences 551162, rat anti-mouse CD45 PE 553081, rat anti-mouse Ly6g PerCP-

275 eFluor710: Thermo-Fisher Scientific 46-9668-82. Samples were incubated with antibody cocktail

276 for 1 hour at 4°C in the dark. After staining, cells were pelleted at 1000 x g for 5 minutes at 4°C.

277 Pellets were washed in 500μL PBS + 1% FBS (Gibco 10437028) and re-pelleted at 1000 x g for

278 5 minutes at 4°C. Cells were resuspended in 4% paraformaldehyde and fixed for 1 hour at room

279 temperature. Fixed cells were subsequently pelleted at 1000 x g for 5 minutes at 4°C, filtered

280 through at 100μm mesh filter, resuspended in PBS + 1% FBS and analyzed on a BD LSRFortessa

281 flow cytometer.

282

283 *Statistical analyses:* All statistical tests were performed on groups with n > 3 in GraphPad Prism

284 v9.0.0. To compare two-groups, student's *t*-tests were used. To compare three or more groups,

285 one-way ANOVA (parametric data) or Kruskal-Wallis (non-parametric data) were used followed

286 by Tukey's (parametric data) or Dunn's (non-parametric data) multiple comparisons tests. To

287 compare grouped data, two-way ANOVA with no correction was performed followed by Tukey's

288 multiple comparison test. To assess statistical differences between Kaplan-Meyer curves, Mantel-

289 Cox log-rank tests were performed.

290

291 **RESULTS:**

292 _Analysis of SARS-CoV-2 VoCs in cell culture:_ Viral propagation of SARS-CoV-2 VoCs relative to

293 ancestral SARS-CoV-2 strains is not fully characterized. Vero E6 cells were infected with WA-1,

294 B.1.1.7, and B.1.351 to investigate whether these VoCs infect cells differently using standard

295 plaque assays and viral growth kinetics. Plaque morphology of SARS-CoV-2 VoC infected

296 cultures was distinct (Figure 1A), with B.1.1.7 resulting in a wider and rounder plaque phenotype

297 relative to WA-1 and B.1.351 infected cells. B.1.351 viral titer was significantly increased 24 hours

298 post-infection in cell culture but declined to levels comparable to B.1.1.7 and WA-1 over 72 hours

299 (Figure 1B-F). To determine the genetic background of the SARS-CoV-2 VoCs used in this study,

300 deep-sequencing was performed, and mutations relative to the WA-1 strain were identified for

301 B.1.1.7 (Supplementary Figure 2A) and B.1.351 (Supplementary Figure 2B) prior to use in both

302 _in vitro_ and K18-hACE2 experiments. Both strains exhibited mutations associated with widely

303 propagating B.1.1.7 and B.1.351 SARS-CoV-2 strains (Rambaut et al., 2020; Tegally et al., 2020).

304 In addition, authentication of B.1.351 stocks used in this study revealed a large deletion in viral

305 ORF7a (Supplementary Figure 3) that was not previously reported.

306

307 _Clinical disease progression of mice infected with SARS-CoV-2 VoCs:_ Enhanced infectivity and

308 divergent genomes of SARS-CoV-2 VoCs found in humans suggests that infection of pre-clinical

309 animal models of SARS-CoV-2 by VoCs may be different. Many features of WA-1 SARS-CoV-2

310 disease progression have previously been described in this model (Hassan et al., 2020; Kumari

311 et al., 2020; Liu et al., 2021; Moreau et al., 2020; Pandey et al., 2020; Sarkar and Guha, 2020;

312 Silvas et al., 2021). K18-hACE2 transgenic mice were infected with SARS-CoV-2 VoCs and

313   assessed daily until moribund (Supplementary Figure 1). Physical assessments of mice were

314   compared using 10^3, 10^4, and 10^5 pfu doses. Temperature (Figure 2A-D) and weight (Figure 2E-

315   H) were monitored for the duration of the infection. Mice infected with the B.1.1.7 strain exhibit

316   earlier hypothermia and weight loss relative to either the B.1.351 or WA-1 VoCs (Figure 2A-D).

317   Hypothermia and weight loss trended higher in the B.1.1.7 VoC infected mice at both 10^4 and 10^5

318   pfu doses at five days post-infection (Figure 2A-H). Clinical scores were assigned to mice (scale

319   described in methods and Supplementary Figure 1) based on their appearance, eye closure,

320   respiration, activity, hypothermia, and weight loss (Supplementary Figure 1) as described

321   previously. B.1.1.7 and B.1.351 VoC infected mice exhibited higher cumulative clinical scores

322   than the WA-1 strain at the 10^3 pfu dose (Figure 2I) and individual clinical scores at five days post-

323   infection increased significantly with viral dose irrespective of the viral strain (Figure 2J). Mice

324   infected with the B.1.1.7 VoC at 10^4 pfu exhibited an increase in clinical score earlier than the

325   B.1.351 and WA-1 strains at the same dose (Figure 2I-J). At later time-points, both VoC presented

326   higher clinical scores than the WA-1 at all the challenging doses studied. Importantly, at 10^3 pfu

327   both VoC presented 100% mortality; however, WA-1 presented 60% survival (Figure 3,

328   Supplementary Figure 4). Mice infected with 10^4 and 10^5 pfu of each VoC succumbed to infection

329   (Figure 3). The WA-1 strain exhibited the largest difference in survival between challenge doses,

330   with approximately 50% of mice recovering from the 10^3 pfu dose (Figure 3, Supplementary Figure

331   4) compared to 0% recovery in B.1.1.7 and B.1.351 challenged groups (Figure 3). Interestingly,

332   mice infected with the B.1.351 SARS-CoV-2 VoC succumbed to infection around 5 days post-

333   infection independently of the challenge dose used (Figure 3). These data demonstrate

334   differences in lethality between VoC doses in the K18-hACE2 transgenic murine host.

335

336   _VoCs escape protection from convalescent plasma:_ Our significant differences observed in the

337   viral genetic sequence, viral replication _in vitro_, and infection _in vivo_, established that SARS-CoV-

338   2 VoC behave differently during infection driving differential outcome. Given the evidence that

339   SARS-CoV-2 VoCs can resist antibody therapeutics (Wang et al., 2021), we next sought to

340   investigate if VoCs may bypass protection from antibodies present in convalescent plasma (CP)

341   from an individual infected with SARS-CoV-2 in March of 2020. K18-hACE2 transgenic mice were

342   intranasally challenged with a lethal dose of 10^5 pfu of SARS-CoV-2 VoCs B.1.1.7, B.1.351, or

343   WA-1 and subsequently treated with CP obtained from an individual infected in March 2020 (WA-

344   1), or from non-SARS-CoV-2 exposed healthy human serum (HHS, confirmed by PCR and

345   serological testing) (Figure 4). IgG levels and nAb data for these sera relative to other serum

346   samples from SARS-CoV-2 infected, non-infected, and a vaccinated human is provided (see

347   Supplementary Figure 5). Mice infected with the B.1.1.7 VoC and WA-1 strain exhibited significant

348   differences in clinical measurements when treated with HHS or CP. Trends in temperature (Figure

349   4A-C), weight loss (Figure 4E-G). and clinical score (Figure 4I) over time were different between

350   HHS and CP treated groups. B.1.1.7 and WA-1 exhibited significantly reduced temperature four

351   days post-infection, B.1.1.7 exhibited significantly reduced weight four days post-infection, and

352   B.1.1.7 and WA-1 exhibited significantly increased clinical scores four days post-infection when

353   treated with HHS compared to CP (Figure 4). All WA-1 infected mice had no temperature or weight

354   loss, and 60% of B.1.1.7 infected mice had no temperature or weight loss when treated with CP

355   (Figure 4A-H). However, all mice infected with the B.1.351 VoC exhibited observable declines in

356   temperature and weight regardless of treatment, suggesting that CP does not adequately protect

357   mice from B.1.351 infection. Survival of mice treated with CP was significantly different than mice

358   treated with HHS for the B.1.1.7 and WA-1 VoCs (Figure 5A-B). CP protected 100% of mice

359   against lethal WA-1 infection and 60% of mice against lethal B.1.1.7 infection. However, no

360   protection was observed in mice infected with the B.1.351 VoC, with 100% of CP-treated infected-

361   mice reaching morbidity one day later (6 days post-infection) than B.1.351 infected mice treated

362   with HHS (5 days post-infection). (Figure 5A-B). CP treatment resulted in decreased viral copy

363   number in the lungs of mice infected with either WA-1 or B.1.1.7, but not mice infected with

364   B.1.351 (Figure 5C). CP treatment only reduced viral copy number in brain tissue of mice infected

365   with WA-1 and not differences in viral titers were observed in mice infected with B.1.1.7 or B.1.351

366   (Figure 5D).

367

368   *Human and mouse IgG levels in convalescent plasma treated K18-hACE2 transgenic mice*

369   *infected with SARS-CoV-2 VoCs:* To determine the level of IgGs delivered to HHS and CP treated

370   mice, we analyzed whether human anti-SARS-CoV-2 IgGs were present within the lung and sera

371   of animals treated with CP or HHS through the course of infection (Figure 6, Supplementary

372   Figure 6). The data demonstrate that significant quantities of human anti-SARS-CoV-2 IgGs

373   targeting both the S RBD and N proteins were present at two days post-infection (Supplementary

374   Figure 6), in sera (Figure 6A, 6C, 6E, 6G) and lung (Figure 6B, 6D, 6F, 6H) at euthanasia of CP-

375   treated mice relative to HHS-treated mice. Relative quantities of anti-SARS-CoV-2 IgGs were

376   similar across CP groups at all time points. A non-significant decrease of anti-N IgGs was

377   observed in the lungs of CP-treated B.1.351 infected mice (Figure 6H). This observation suggests

378   that there may be a greater prevalence of free N antigen in the lung that is decreasing the anti-N

379   IgG titer. These data demonstrate successful administration of anti-SARS-CoV-2 IgGs to CP-

380   treated mice.

381

382   *Immunological response to VoC infection and treatment with convalescent plasma:* Next, we

383   assessed cytokine levels in K18-hACE2 transgenic mice infected with SARS-CoV-2 VoCs. Serum

384   from animals at 2 days post-infection and at euthanasia, or supernatants from lung homogenates

385   were tested for the presence of Th1 (TNF, IL-2). Thh2 (IL-6, IL-10, IL-13), inflammasome (IL-1β)

386   and regulatory (IL-27) cytokines (Figure 7, Supplementary Figure 7). We assayed these cytokines

387   as many are established as pro-inflammatory mediators that are upregulated during SARS-CoV-

388   2 infection (Hojyo et al., 2020; Horspool et al., 2021; Oladunni et al., 2020; Ye et al., 2020b) or

389   are involved in the response to viral encephalitis (Angioni et al., 2020; Aquino et al., 2021; Fabbi

390   et al., 2017; Oladunni et al., 2020), including K18 hACE2 transgenic mice. CP treatment reduced

391   IL-6, TNF-α, IFN-γ, IL-10 and IL-27 in B.1.351 infected mice, and IL-6 in B.1.1.7 two days post

392   infection (Figure 7A-E). This trend was abrogated or reversed in B.1.351 infected mice at

393   euthanasia (Figure 7F-J). Limited differences were observed in cytokine expression in the lung,

394   except decreased TNF-α in the lungs of CP-treated mice infected with WA-1 (Figure 7K-O). Minor

395   or no differences were detected in IL-1β, IL-2, IL-13, and IL-17 at two days post-infection,

396   euthanasia, or in the lung (Supplementary Figure 7). To understand the cellular response to

397   infection, we analyzed T cells and myeloid cells in the lungs of K18-hACE2 transgenic mice

398   infected with SARS-CoV-2 VoCs. B.1.351 infected mice exhibited significantly increased T-cell

399   ($CD3^+$ or $CD4^+$) recruitment to the lungs relative to WA-1 infected mice (Supplementary Figure

400   8A-B). Non-significant trends in $CD8^+$ T cells and myeloid cells were observed but further studies

401   defining their function will be required (Supplementary Figure 8C-F).

402

403   **DISCUSSION:** SARS-CoV-2 VoCs of concern are rapidly evolving and some are exerting

404   dramatic negative impacts on the currently ongoing COVID-19 pandemic. The goal of this study

405   was to gain information regarding the infectivity of SARS-CoV-2 VoCs in *in vitro* and *in vivo* using

406   the validated K18 hACE2 transgenic mouse model of SARS-CoV-2 infection. Our data present a

407   broad picture suggesting that the VoCs exhibit major differences in pathogenesis, immune

408   activation, and lethality in the K18-hACE2 transgenic mouse model of infection. B.1.351 replicated

409   faster in cell culture than B.1.1.7 and WA-1. Both B.1.1.7 and B.1.351 triggered severe clinical

410   indications of disease at lower infectious doses than the ancestral WA-1 strain in the K18-hACE2

411   transgenic murine model. Treatment of infected mice with CP from WA-1-infected individuals

412   (March of 2020, prior to the emergence of B.1.1.7 and B.1.351 VoC) resulted in full protection

413   only against the WA-1; B.1.1.7 infected mice exhibited partial protection and B.1.351 exhibited no

414   protection. Both VoCs resulted in significant viral replication in the brain of K18-hACE2 transgenic

415   mice despite treatment with CP. It is clear by comparing all results from this study (Supplementary

416   Figure 9) that CP efficacy is significantly reduced against SARS-CoV-2 VoC and that antibodies

417 against ancestral SARS-CoV-2 may not be fully protective against B.1.1.7 and B.1.351. This may

418 have additional impacts on the efficacy of existing SARS-CoV-2 vaccines that target the S protein

419 of WA-1 SARS-CoV-2. Ultimately, these results provide a troubling picture of the impact of VoCs

420 on SARS-CoV-2 pathogenesis and host immunity.

421 SARS-CoV-2 B.1.351 infection resulted in unique phenotypes in this study: increased

422 replication in cell culture, clinical presentations at low doses of infection, lethality at low infectious

423 doses, reduced clinical and survival benefits from early (WA-1) CP, increased viral load in lung

424 and brain tissues, and increased pro-inflammatory cytokines after CP treatment, all supporting

425 the conclusion that the B.1.351 VoC results in more severe disease than the original WA-1 strain

426 in this model. Of particular concern is the lack of reduction in viral copy number in all mice treated

427 with CP infected with B.1.351 relative to WA-1 infected mice. In addition, the severity of viral

428 burden despite CP treatment was enhanced in B.1.351 infected mice relative to B.1.1.7 infected

429 mice: 100% of CP-treated B.1.351 infected mice had lung and brain infection relative to 40% of

430 CP-treated B.1.1.7 infected mice. This demonstrates that B.1.351 infection may harbor more

431 resistance or tolerance to early pandemic CP than B.1.1.7. It is important to point out the caveat

432 that we did not investigate antibody dependent enhancement of infection. The observed

433 differences in our mouse challenge studies may be attributable to the alterations in the viral

434 B.1.351 S RBD region of the S protein, which may increase affinity for the hACE2 receptor

435 (Bozdaganyan et al., 2021; Laffeber et al., 2021; Ozono et al., 2021; Shah et al., 2020; Tian et

436 al., 2021) and could result in increased infectivity and pathogenicity. Although this yet speculative,

437 sequencing results in Supplementary Figure 2-3 illustrate that many other mutations exist within

438 the B.1.351 SARS-CoV-2 genome. Mutations within other viral proteins, particularly those

439 involved in viral replication and genome packaging may provide additional advantages for this

440 VoC during infection. It is currently unknown what impact the B.1.351 ORF7a deletion we

441 observed has on pathogenesis, but other studies have suggested limited impacts of similar

442 ORF7a mutations in cell culture (Chiem et al., 2020; Narayanan et al., 2008; Sims et al., 2005).

443 Dissecting the consequences of these B.1.351 non-S mutations will be useful in determining the

444 mechanisms behind the increased disease severity observed here and may help better inform

445 containment of these VoCs, and others emerging in the future.

446   Several additional observations were made in this study, including discovering significant

447 differences in cytokine production of B.1.351 SARS-CoV-2 VoC infected mice. IL-27 is an

448 indicator of acute encephalitis and can activate CD8+ T cells (Angioni et al., 2020; Aquino et al.,

449 2021; Fabbi et al., 2017) in addition to several other less characterized functions (Awasthi et al.,

450 2007; Iwasaki et al., 2013; Jung and Robinson, 2014; Kastelein et al., 2007; Seman et al., 2020;

451 Sugiyama et al., 2008). IL-27 also regulates IL-10 production, the latter acting in an anti-

452 inflammatory manner by suppressing inflammatory responses (Iyer and Cheng, 2012). IL-27 was

453 increased in B.1.351 infected mice. B.1.351 challenged mice also had significant viral burden in

454 the brain, increased $CD3^+$ T cells in the lung, and non-significantly increased in CD8+ T cells in

455 the lung. The combination of these data suggests that IL-27 expression in B.1.351 infected mice

456 may be linked to more severe encephalitis and potentially higher activation of $CD8^+$ T cells. HHS-

457 treated mice infected with B.1.351 exhibited this increase in IL-27 at two days post-infection,

458 whereas CP-treated mice exhibited this increase only at euthanasia. It is possible that this delay

459 in increased IL-27 may be beneficial as CP-treated B.1.351 infected mice survive for one

460 additional day over HHS-treated mice. Mechanistically, this may be due to IL-27 promoting

461 uncontrolled inflammation (Takeda et al., 2003) and suppression of T_{regs} (Cox et al., 2011) which

462 may increase local and systemic damage. However, IL-27 could also be increased as an

463 emergency response in response to encephalitic infection and may exert beneficial pro- or anti-

464 inflammatory effects dependent on the severity of infection. Further studies will be required to

465 elucidate the true role of IL-27 in this system. In a similar manner, IL-6, TNF, and IFN-γ were

466 increased in B.1.351 infected mice two days post-infection in HHS-treated mice and increased in

467 CP-treated mice at euthanasia. This delay in induction of pro-inflammatory cytokines may be

468 beneficial, but ultimately none of these delays appear to protect mice from death.

469   This study also provides additional insights on VoC pathogenicity; however, several

470   important clarifications must be made when interpreting these results. Firstly, although these

471   infection models exhibit clear differences in infectivity, infections in cell culture and mice do not

472   perfectly represent those in humans. In particular, the K18-hACE2 transgenic mouse model is a

473   lethal disease model, with different viral tropism, which frequently can result in 100% mortality at

474   low infectious doses as seen in this study and others (Hassan et al., 2020; Kumari et al., 2020;

475   Liu et al., 2021; Moreau et al., 2020; Oladunni et al., 2020; Pandey et al., 2020; Sarkar and Guha,

476   2020; Silvas et al., 2021). Human disease can range from mild disease to lethal disease and is

477   impacted by comorbidities (Elezkurtaj et al., 2021; Mehra et al., 2020; Wu and McGoogan, 2020).

478   Re-creating this in any animal model is exceptionally challenging. Another complex component is

479   that it is unknown what the minimum infectious dose of SARS-CoV-2 is for humans, and thus it is

480   difficult to compare animal models of infection to a real human infection without this basic

481   information. Secondly, the K18-hACE2 transgenic mouse expresses hACE2 but also retains

482   expression of murine (m)ACE2. There is speculation that SARS-CoV-2 VoCs can infect wild-type

483   mice and cause non-lethal disease by binding to mACE2 (Montagutelli et al., 2021); this may

484   impact the comparisons provided in this study. We have observed similar phenomena in

485   preliminary studies where some of these VoC are able to infect wild-type mice, contrary to the

486   situation with WA-1 strain (data not shown). Although this may be true, infection of Vero E6 cells

487   with B.1.351 (a non-human cell line that is not genetically modified for infection) was significantly

488   increased 24 hours post-infection. This provides support of the conclusions presented here in

489   light of the potential for VoCs to bind mACE2, although an effect of mACE2 cannot be excluded.

490   CP as a treatment has been used widely since the onset of the COVID-19 pandemic

491   (Bloch, 2020; Bloch et al., 2020; Chen et al., 2020), but its efficacy has recently been re-evaluated

492   under certain conditions (Casadevall et al., 2021; Cele et al., 2021; NIH, 2021; Zhao and He,

493   2020). It is possible that some of the decreased efficacy of CP in this study (and others) may be

494   due to SARS-CoV-2 VoCs, and the data presented here support this theory. Other factors

495   including lack of adequate screening for nAbs and lot-to-lot variability of plasma samples may be

496   the cause of these differences in larger studies of humans treated with CP. The plasma used in

497   this study was determined to have high levels of IgG antibodies against SARS-CoV-2 S RBD and

498   N proteins and also exhibited neutralizing activity similar to a vaccinated individual

499   (Supplementary Figure 4). In this context, this plasma should have high protective capacity, and

500   indeed protected WA-1 infected mice against severe disease. Consequently, it is concerning that

501   protection is limited or absent when K18-hACE2 transgenic mice were challenged with B.1.1.7 or

502   B.1.351 VoCs, respectively. It is important to note that only one CP sample was tested in this

503   study and was obtained from a naturally infected, not a vaccinated, individual. Therefore, although

504   there appears to be a lack of protective capacity of this plasma against B.1.351 and partial

505   protective capacity against B.1.1.7, these data do not provide direct against the efficacy of SARS-

506   CoV-2 vaccines which stimulate broader immune responses. However, it is likely that the

507   production of antibodies elicited by existing SARS-CoV-2 vaccines are not fully protective against

508   VoCs, which warrants caution. Further analyses of these vaccines will be critical in determining

509   their efficacy against B.1.1.7, B.1.351, new VoCs, or variants of high concern. Continued support

510   for novel vaccine development against VoCs will be instrumental in providing full protection

511   against evolving strains of SARS-CoV-2.

512   To summarize, this study provides early insight into differences in SARS-CoV-2 VoC

513   pathogenicity in K18-hACE2 transgenic mice and the efficacy of CP containing antibodies

514   targeting WA-1 SARS-CoV-2 against newly emerged SARS-CoV-2 VoCs in the K18-hACE2

515   transgenic mouse model. This study demonstrates increased disease pathology for mice infected

516   with B.1.1.7 and B.1.351 VoCs and lack or limited protection from CP in mice infected with B.1.351

517   and B.1.1.7, respectively. Immunological profiles were different between mice infected with each

518   VoC, with B.1.351 stimulating greater increases in cytokine levels and potential T-cell recruitment,

519   most likely due to its more efficient replication as compared to the WA-1 and B.1.1.7 strains.

520   Overall, these data present a concerning picture of the SARS-CoV-2 VoCs warranting continued

521   caution as the pandemic continues and evolves and suggest the need to update current vaccines

522   to protect against these newly emerged SARS-CoV-2 VoC.

523

534

535   **AUTHOR CONTRIBUTIONS:** A.M.H, F.H.D, I.M, J.T, C.Y and L.M.S designed the experiments.

536   C.Y performed *in vitro* analyses of SARS-CoV-2 VoCs, and J.S., A.G, and R.K.P performed

537   sequencing. M.T.W and I.M propagated virus for animal experiments. A.M.H, T.Y.W, B.P.R, K.S.L

538   and F.H.D infected and euthanized animals, dissected organs, and prepared them for analyses.

539   A.M.H and B.P.R performed ELISA against SARS-CoV-2 antigens and A.M.H and T.Y.W

540   performed qPCR to determine viral load. A.M.H performed cytokine analyses. A.M.H and T.Y.W

541   prepared cells for flow cytometry and A.M.H performed flow cytometry and analysis. J.D analyzed

542   sequence data from viral passages used for infection of K18-hACE2 transgenic mice. A.M.H

543   analyzed, formatted, and represented data for publication. H.A.C assisted with general revisions.

544   All authors contributed to the writing and revision of the manuscript.

545

546 **DECLARATION OF INTERESTS:** The authors declare no competing interests.

547

548 **FIGURES:**

549
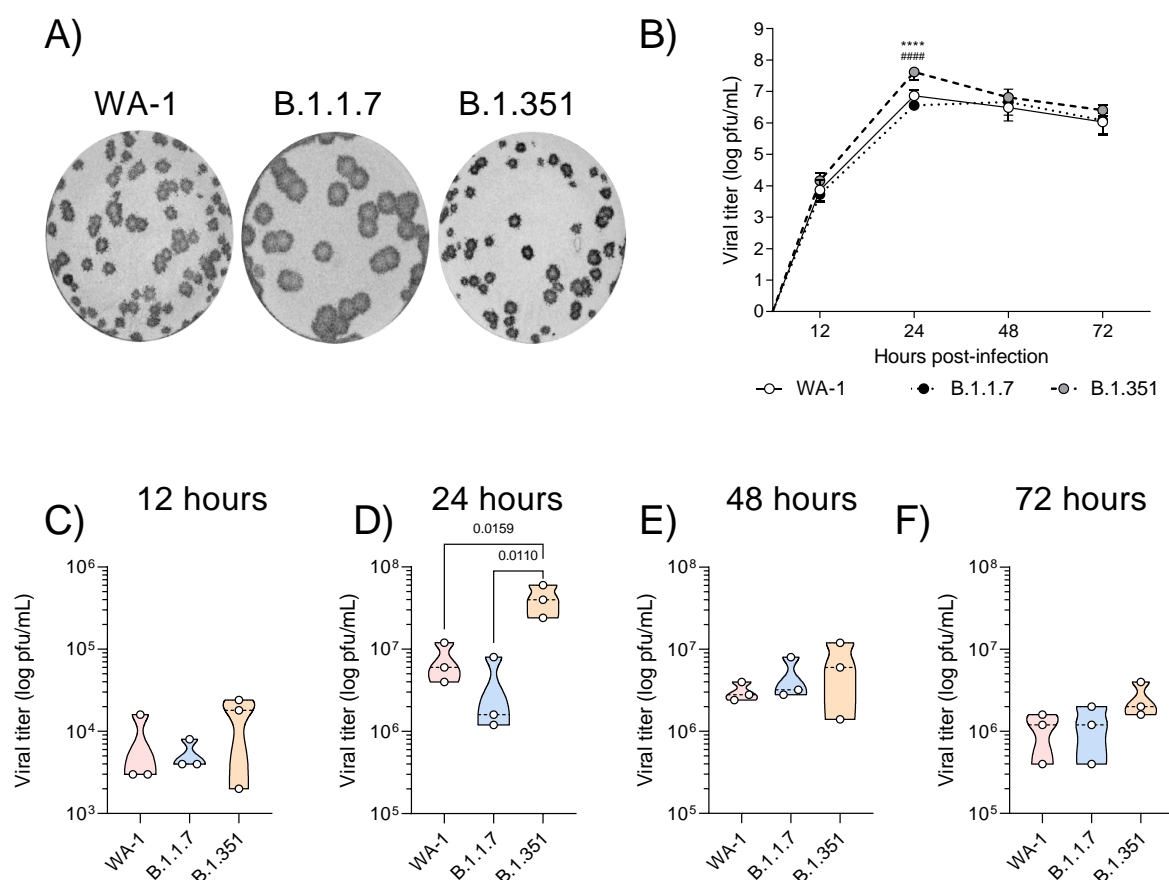
550 **Figure 1 | Characterization of SARS-CoV-2 variants *in vitro*:** (A) Plaque morphology of SARS-

551 CoV-2 WA-1, B.1.1.7 or B.1.351 infected VeroE6 cells. (B) Quantification of viral replication of

552 SARS-CoV-2 variants in VeroE6 cells over time was quantified. Comparison of viral titers in cell

553 culture at 12 (C), 24 (D), 48 (E), and 72 (F) hours post-infection. Statistical analysis of viral

554 replication was completed by two-way ANOVA followed by Tukey's multiple comparison test, or

555 RM ANOVA followed by Tukey's multiple comparison test. **** = $P < 0.0001$ relative to WA-1, ####

556 = $P < 0.0001$ relative to B.1.1.7.
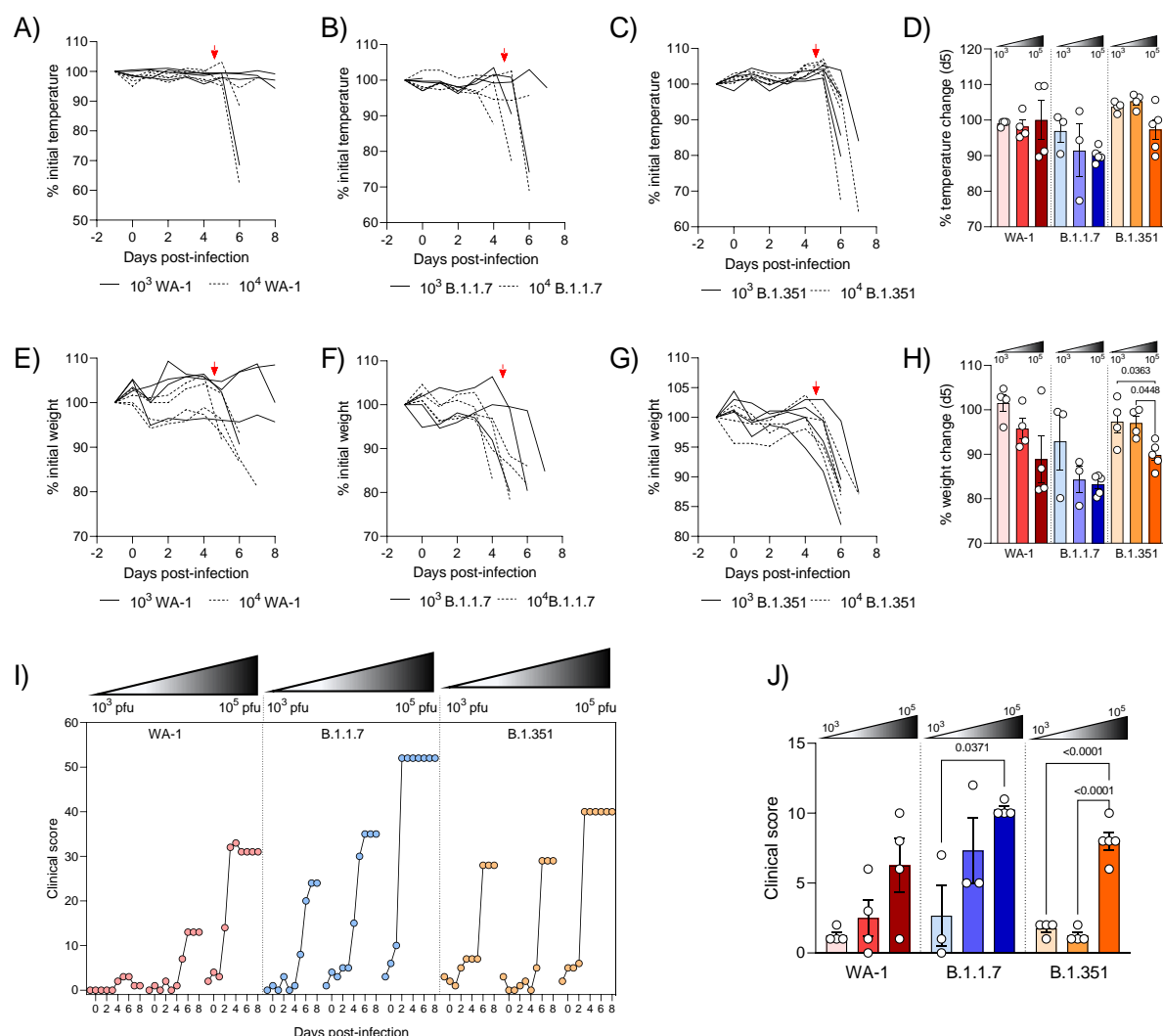
Figure 2 | Establishing clinical endpoints of SARS-CoV-2 VoC infection in K18-hACE2 transgenic mice: Mice were infected with 10^3, 10^4 or 10^5 pfu of SARS-CoV-2 VoCs and were monitored for temperature (A-C), body weight (E-G), and clinical score (I-J) changes over infection. Temperature (D), body weight (H), and clinical scores (J) on day 5 post-infection were assessed. If mice were deceased at five days post-infection, their clinical data at time of euthanasia is presented. Arrows indicate day 5 (A-H). Statistical significance was assessed by one-way ANOVA followed by Tukey's multiple comparison test. n > 3 subjects per group.

566
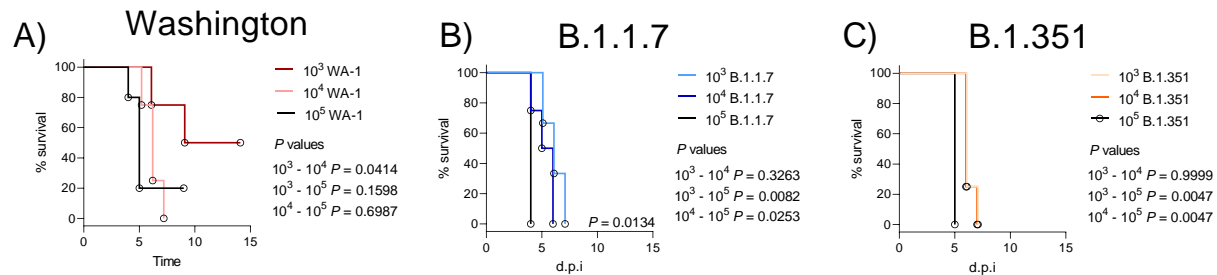
567 **Figure 3 | Impact of dose on survival of K18-hACE2 transgenic mice infected with SARS-**

568 **CoV-2 VoCs:** Kaplan-Meyer survival curves of mice infected with WA-1 (A), B.1.1.7 (B), or

569 B.1.351 (C) VoCs at 10^3, 10^4, and 10^5 pfu doses. Statistical significance was assessed by Mantel-

570 Cox tests. n = 3-5 subjects per group. *P* values for significant differences are reported.

571
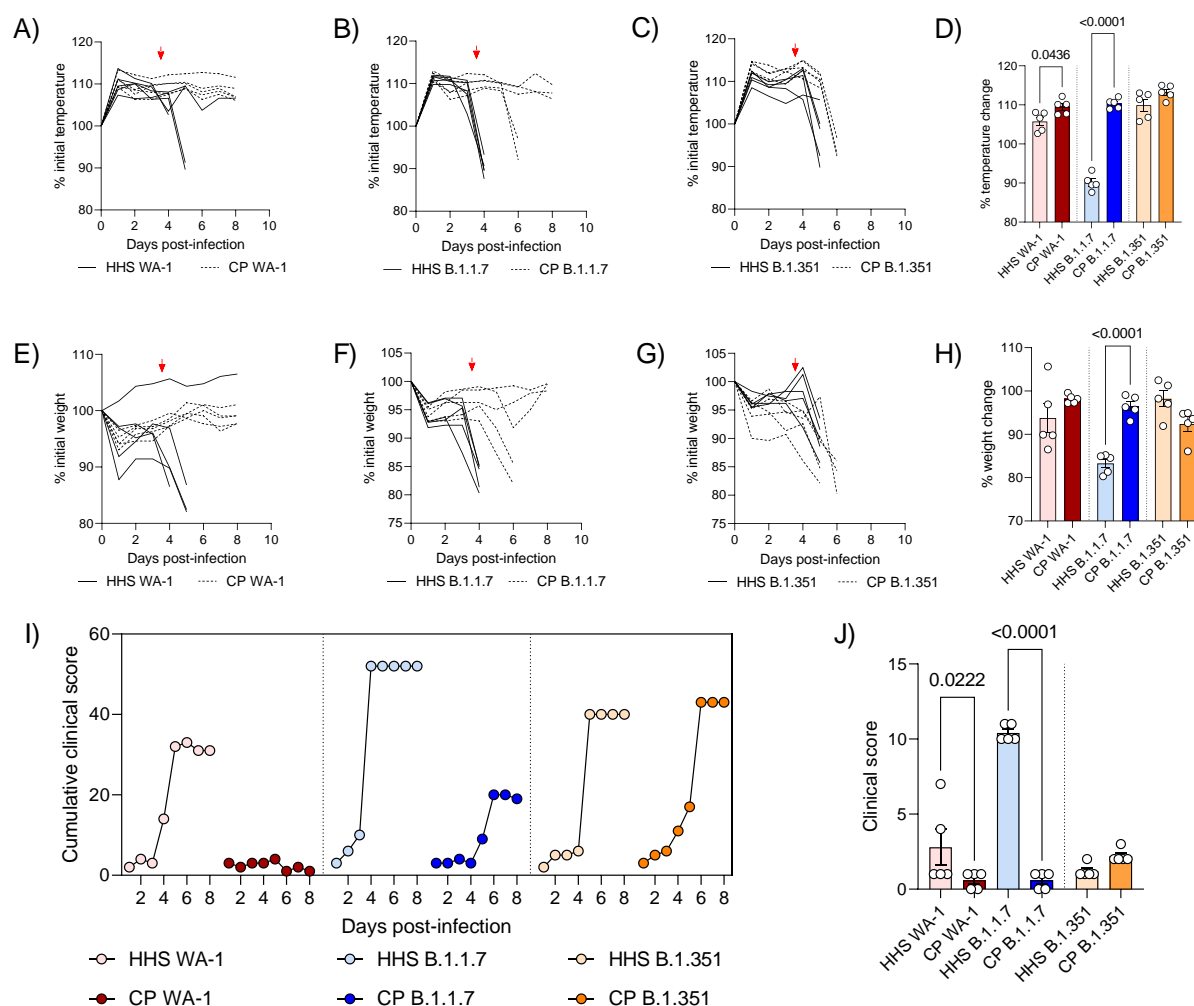
Figure 4 | Effect of convalescent plasma treatment on SARS-CoV-2 VoC infection in K18-hACE2 transgenic mice: Mice infected with 10^5 pfu SARS-CoV-2 VoCs were treated intraperitoneally with 500µL HHS or CP and monitored for temperature (A-C), body weight (E-G) and clinical score (I) over the course of infection. Temperatures (D), body weights (H), and clinical scores (J) on day 4 post-infection were assessed. Arrows indicate day 4 (A-H). Statistical significance was assessed by one-way ANOVA followed by Tukey's multiple comparison test. n > 3 subjects per group. *P* values for significant differences are reported.

581
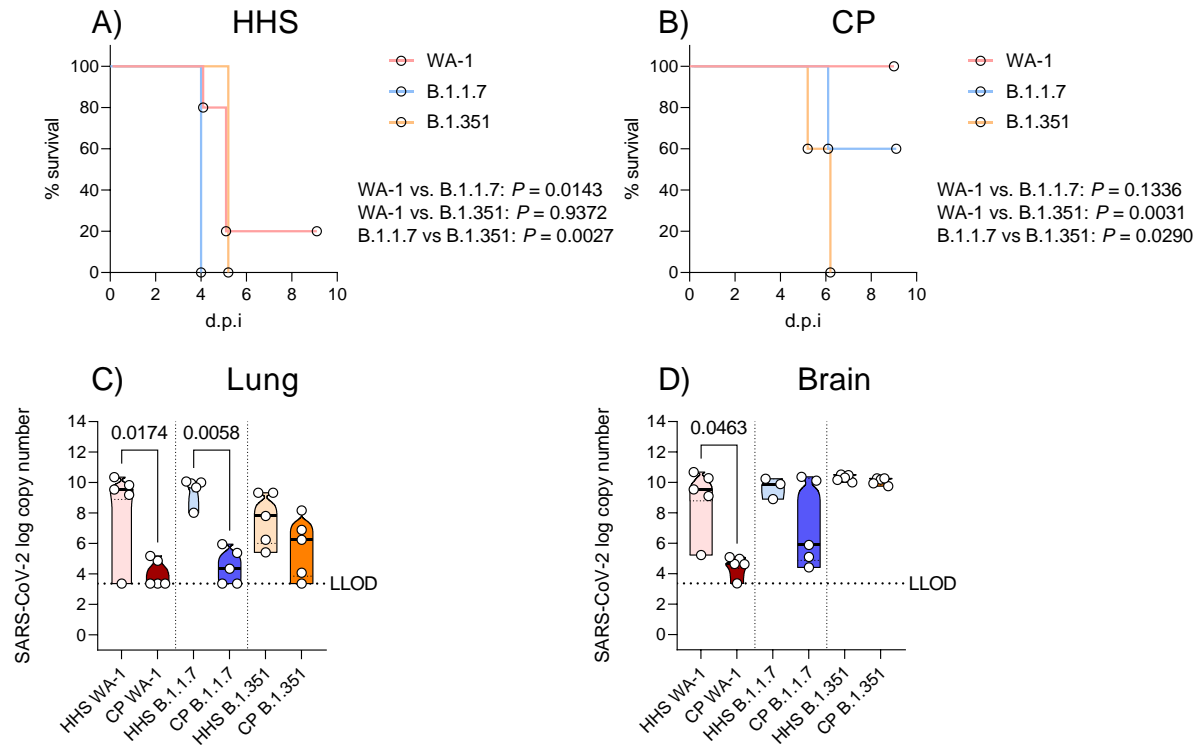
Figure 5 | Survival and viral infection of serum-treated K18-hACE2 transgenic mice infected with SARS-CoV-2 VoCs: Kaplan-Meyer survival curves of mice infected with B.1.1.7, B.1.351, or WA-1 treated with HHS (A) or early pandemic SARS-CoV-2 CP (B). Viral copy numbers in the lung (C) and brain (D) of infected mice. LLOD = lower limit of detection based on a standard curve. Statistical significance of survival curves was assessed with the Mantel-Cox test. Statistical significance between viral copy number was assessed by a Kruskal-Wallis test followed by Dunn's multiple comparisons test. n > 3 subjects per group. *P* values for significant differences are reported.

590
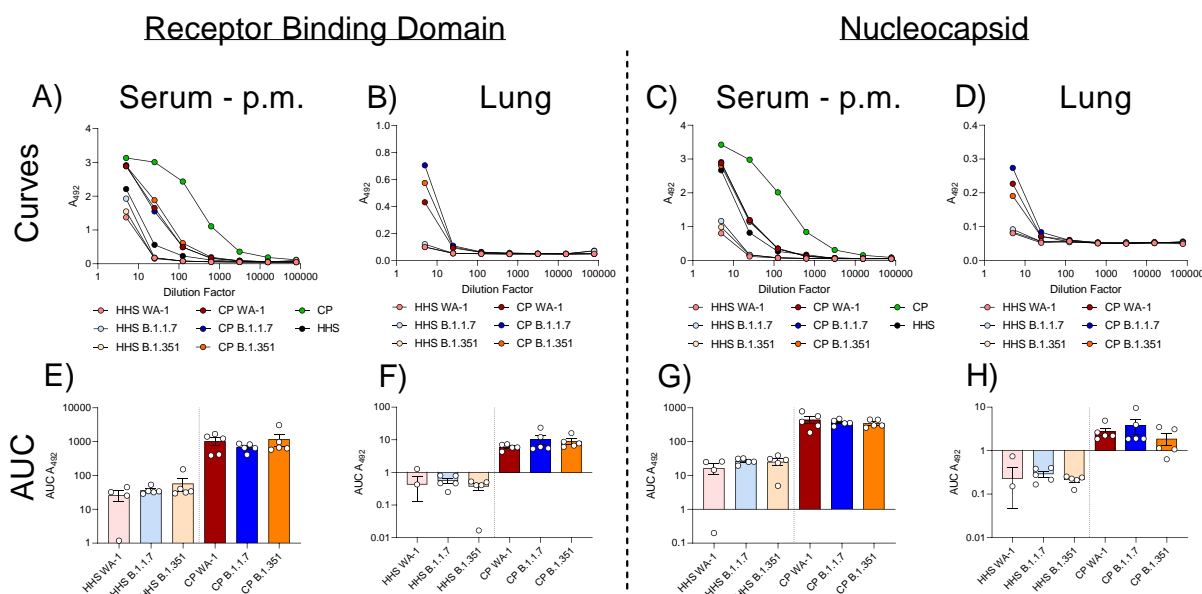
Figure 6 | Human anti-SARS-CoV-2 IgGs in serum-treated K18-hACE2 transgenic mice infected with SARS-CoV-2 VoCs: Human antibody (IgG) levels against SARS-CoV-2 antigens. Anti-RBD curves in serum (A) and lung (B) or anti-N curves in serum (C) or lung (D) of infected mice. Area under the curve (AUC) analyses of anti-RBD IgG levels in the serum (E) or lung (F) of infected mice. AUC analyses of anti-N IgG levels in the serum (G) or lung (H). Statistical significance between AUCs was assessed by a Kruskal-Wallis test followed by Dunn's multiple comparisons test. . n > 3 subjects per group.
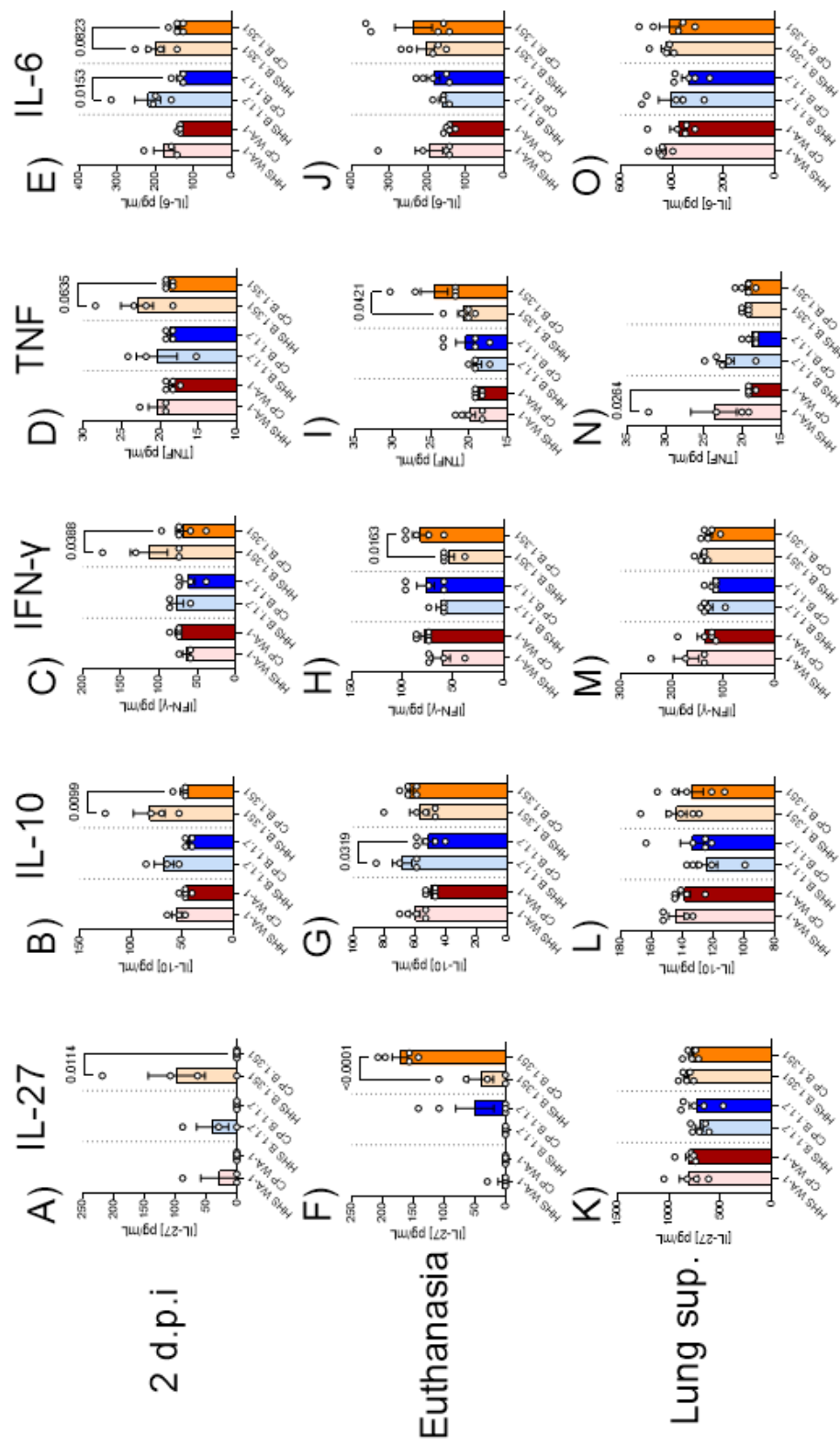
Figure 7 | Cytokine responses in serum-treated K18-hACE2 transgenic mice: IL-6, TNF-a, IFN-y, IL-10, and IL-27 were quantified in serum two days post infection (A-E), in serum at euthanasia (F-J), or in the lung (K-O). Statistical significance was assessed by one-way ANOVA followed by Tukey's multiple comparison test. n > 3 subjects per group. *P* values for significant differences are reported.
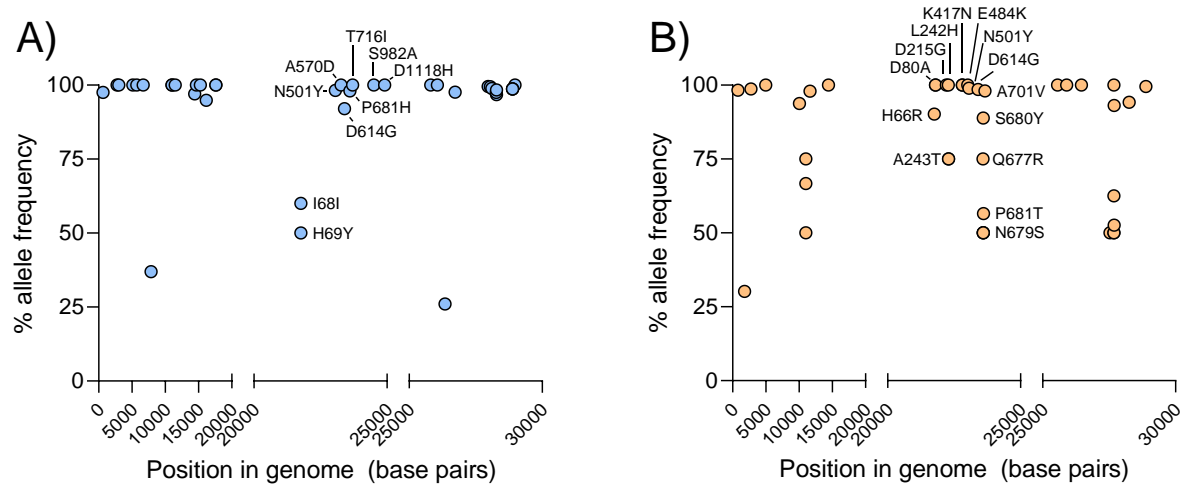
600

601

602 **SUPPLEMENTARY FIGURES:**

603

604 **Supplementary Figure 1 | Clinical scoring system:** K18-hACE2 transgenic mice were

605 assessed for weight loss, appearance, activity, eye closure, respiration, and temperature and

606 scored using the metrics provided. Mice with a score of 5 in weight loss or a 2 in respiration were

607 euthanized.

Supplementary Figure 2 | Sequencing of SARS-CoV-2 VoCs in this study: NGS of SARS-CoV-2 WT and VoCs demonstrates that mutations associated with each variant are present within the B.1.1.7 (A) and B.1.351 (B) genomes. Mutations within the spike protein are labeled.

```
ORF7a_Washington_MN985325.1        1  MKIILFLALITLATCELYHYQECVRGTTVLLKEPCSSGTYEGNSPFHPLADNKFALTCFS
ORF7aDEL_South_Africa_NR-54008     1  MKIILFLALITLATCELYHYQECVRGTTVLLKEPCSSGTYEGNSPFQ.............


ORF7a_Washington_MN985325.1       61  TQFAFACPDGVKHVYQLRARSVSPKLFIRQEEVQELYSPIFLIVAAIVFITLCFTLKRKT
ORF7aDEL_South_Africa_NR-54008    48  .......................................IFLIVAAIVFITLCFTLKRKT


ORF7a_Washington_MN985325.1      121  E
ORF7aDEL_South_Africa_NR-54008    69  E
```

613

Supplementary Figure 3 | ORF7a deletion in B.1.351 SARS-CoV-2 VoC in this study:

Annotated deletion within the ORF7a protein of the B.1.351 VoC used in this study.

616
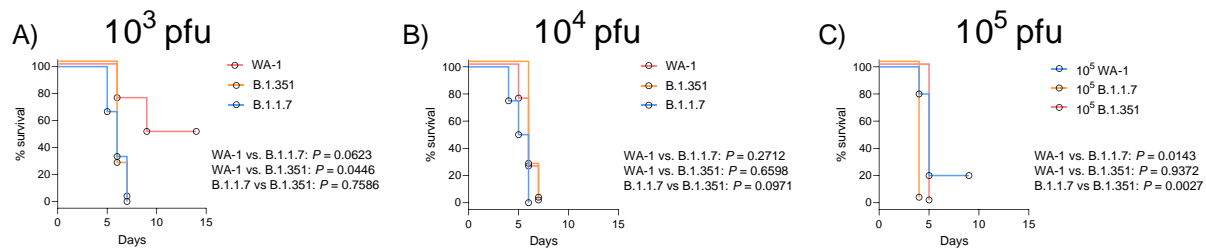
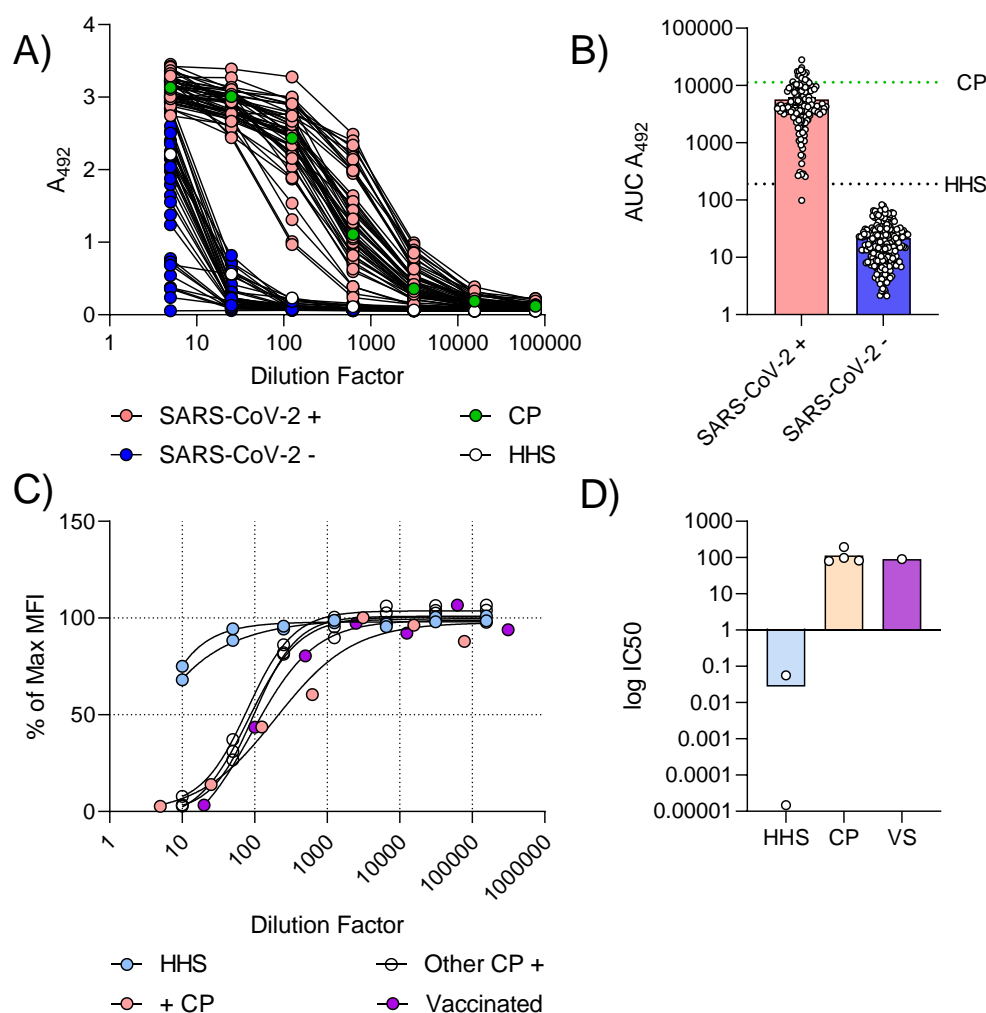**Supplementary Figure 4 | Impact of variant on survival of K18-hACE2 transgenic mice infected with SARS-CoV-2 VoCs :** Kaplan-Meyer survival curves of mice infected with 10^3 (A), 10^4 (B), or 10^5 (C) pfu doses of WA-1 B.1.1.7, or B.1.351 SARS-CoV-2 VoCs. Statistical significance was assessed by Mantel-Cox tests. n > 3 subjects per group. *P* values for significant differences are reported.

624

Supplementary Figure 5 | Anti-RBD IgG levels and neutralization capacity of HHS and CP:

IgG levels of CP and HHS were assessed using ELISA developed previously. CP (green, dotted green line) and HHS (white, dotted black line) ELISA curves (A) and AUCs (B) were compared to a subset of SARS-CoV-2$^+$ (red) and SARS-CoV-2$^-$ (blue) individuals from a prior study. Neutralizing antibody function was assessed with a modified Luminex assay. Neutralization curves (C) and IC50 values (D) for nAbs from HHS (blue), CP (red), and a vaccinated individual (purple) are provided.

632

633
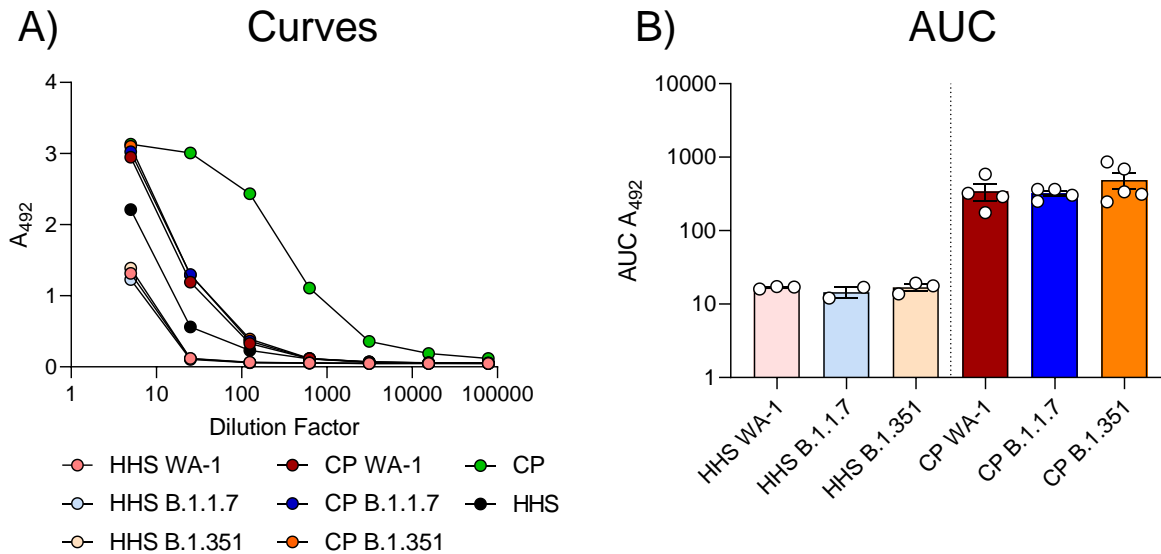
Supplementary Figure 6 | Human anti-SARS-CoV-2 IgGs two days post-infection in serum-treated K18-hACE2 transgenic mice infected with SARS-CoV-2 VoCs: Antibody (IgG) level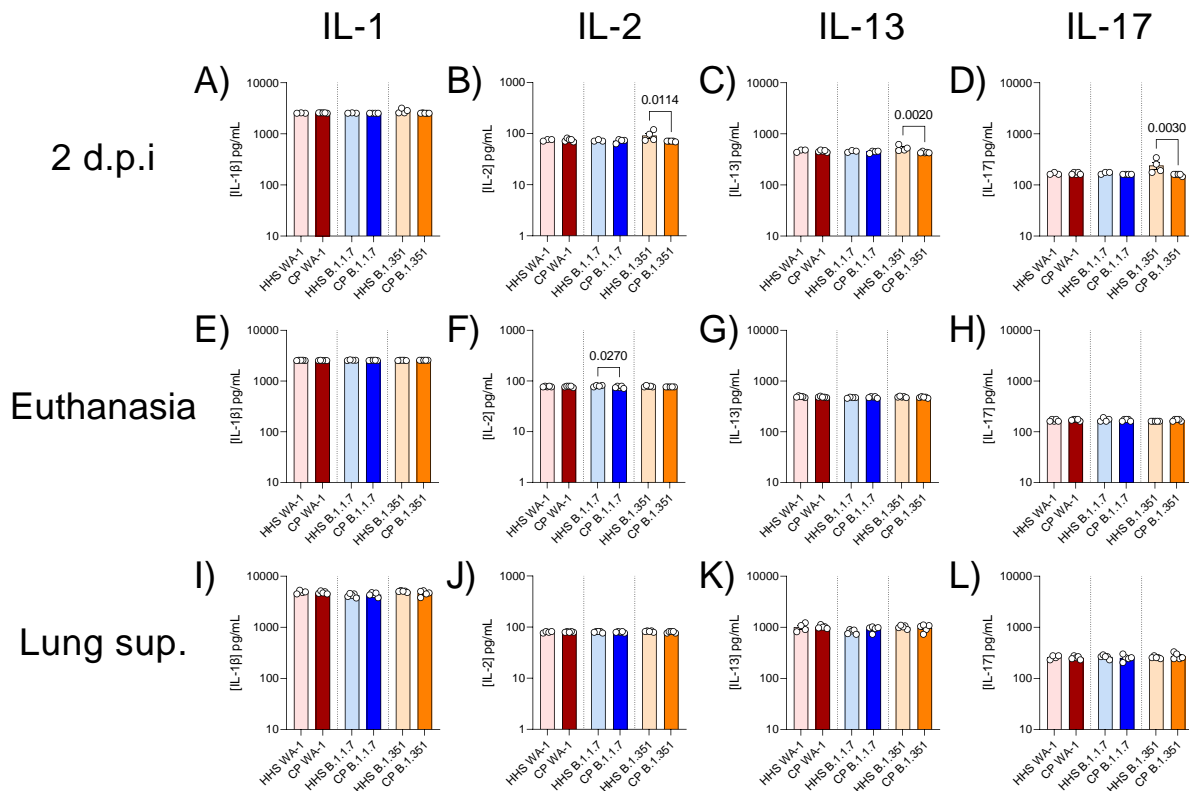s against SARS-CoV-2 antigens. Anti-RBD curves in serum (A) and of infected K18-hACE2 transgenic mice 2 days post-infection. Area under the curve (AUC) analyses of anti-RBD IgG levels (B). Statistical significance between AUCs was assessed by a Kruskal-Wallis test followed by Dunn's multiple comparisons test. n > 3 subjects per group.

640

641

Supplementary Figure 7 | Minor or no differences in some cytokine levels in K18-hACE2 transgenic mice treated with serum: IL-1, IL-2, IL-13, and IL-17 were quantified in serum two days post infection (A-D), in serum at euthanasia (E-H), or in the lung (I-L). Statistical significance was assessed by one-way ANOVA followed by Tukey's multiple comparison test. n > 3 subjects per group. *P* values for significant differences are reported.

647
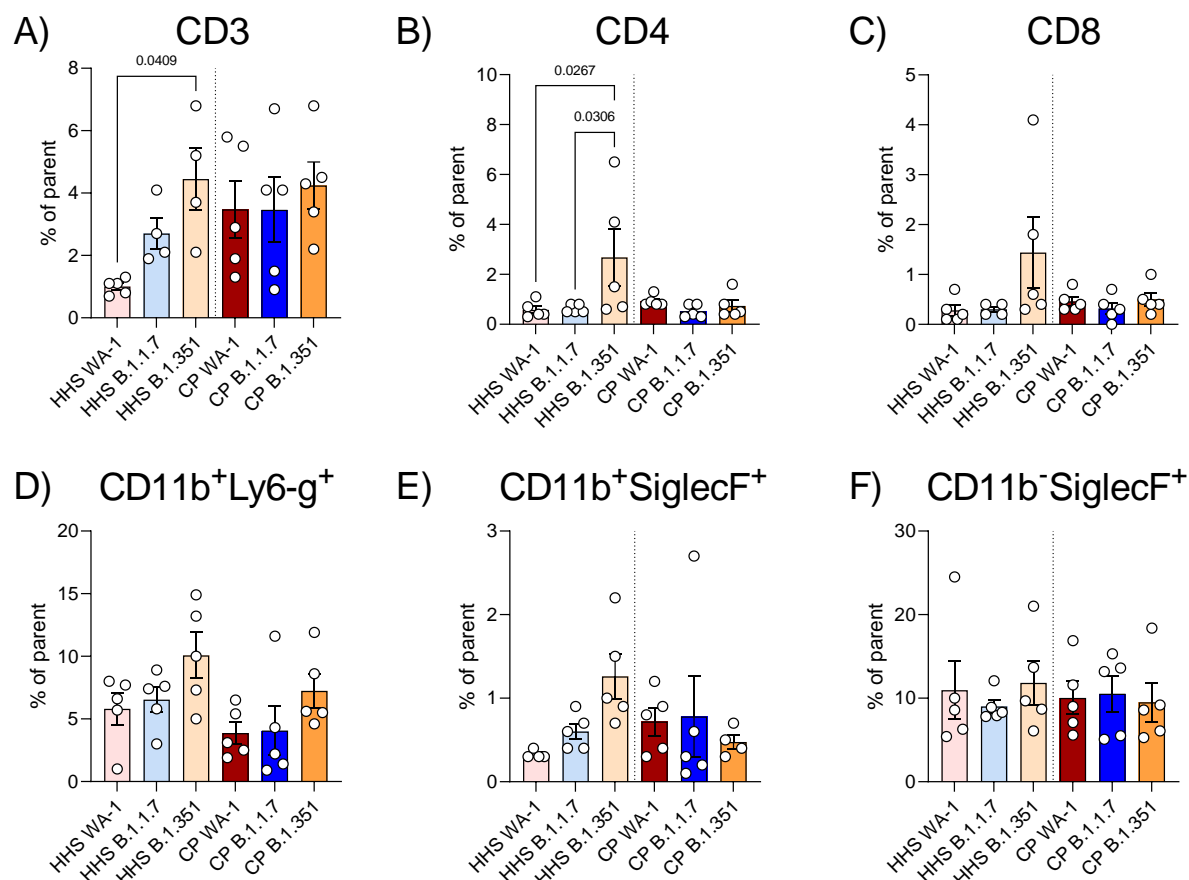
Supplementary Figure 8 | T cell and myeloid cell populations in lungs of K18-hACE2 transgenic mice infected with SARS-CoV-2 VoCs: CD3 (A), CD4 (B), and CD8 (C) T cells were quantified in lung homogenates from SARS-CoV-2 variant infected K18-hACE2 transgenic mice. CD11b$^+$Ly6-g$^+$ (D), CD11b$^+$SiglecF$^+$, and CD11b$^-$SiglecF$^+$ cells myeloid cells were also quantified in lung homogenates. Statistical analyses were performed by one-way ANOVA followed by Tukey's multiple comparison test. n>3 samples per group. *P* values of statistically significant results are reported.
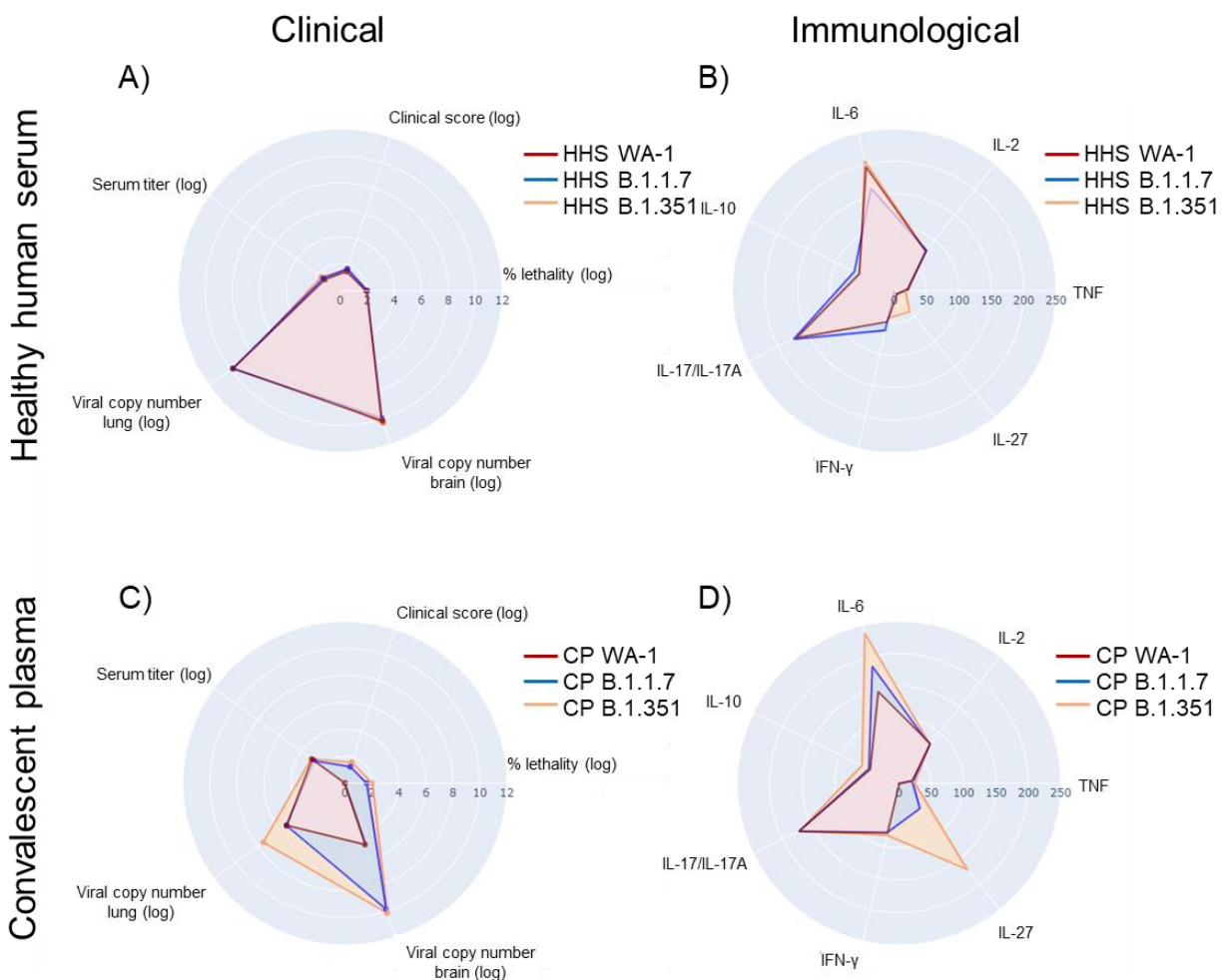
Supplementary Figure 9 | Comparison of clinical and immunological phenotypes of SARS-CoV-2 infected K18-hACE2 transgenic mice treated with HHS or CP: Clinical (A) and immunological (B) phenotypes of SARS-CoV-2 infected K18-hACE2 transgenic mice treated with HHS. Clinical (C) and immunological (D) phenotypes of SARS-CoV-2 infected K18-hACE2 transgenic mice. Scatterpolar plots were generated in Python using plotly.

REFERENCES:

Addetia, A., Crawford, K.H.D., Dingens, A., Zhu, H., Roychoudhury, P., Huang, M.L., Jerome, K.R., Bloom, J.D., and Greninger, A.L. (2020). Neutralizing antibodies correlate with protection from SARS-CoV-2 in humans during a fishery vessel outbreak with high attack rate. MedRxiv *58*, 1–11.

Angioni, R., Sánchez-rodríguez, R., Munari, F., Bertoldi, N., Arcidiacono, D., Cavinato, S., Marturano, D., Zaramella, A., Realdon, S., Cattelan, A., et al. (2020). Age-severity matched cytokine pro fi ling reveals speci fi c signatures in Covid-19 patients.

Aquino, M.T.P. De, Kapil, P., Hinton, D.R., Phares, T.W., Puntambekar, S.S., Bergmann, C.C., and Stohlman, S.A. (2021). IL-27 Limits Central Nervous System Viral Clearance by Promoting IL-10 and Enhances Demyelination.

Awasthi, A., Carrier, Y., Peron, J.P.S., Bettelli, E., Kamanaka, M., Flavell, R.A., Kuchroo, V.K., Oukka, M., and Weiner, H.L. (2007). A dominant function for interleukin 27 in generating interleukin 10-producing anti-inflammatory T cells. Nat. Immunol. *8*, 1380–1389.

Bloch, E.M. (2020). Convalescent plasma to treat COVID-19. Blood *136*, 654–655.

Bloch, E.M., Shoham, S., Casadevall, A., Sachais, B.S., Shaz, B., Winters, J.L., Van Buskirk, C., Grossman, B.J., Joyner, M., Henderson, J.P., et al. (2020). Deployment of convalescent plasma for the prevention and treatment of COVID-19. J. Clin. Invest. *130*, 2757–2765.

Bolger, A.M., Lohse, M., and Usadel, B. (2014). Genome analysis Trimmomatic : a flexible trimmer for Illumina sequence data. *30*, 2114–2120.

Bozdaganyan, M.E., Sokolova, O.S., Shaitan, K. V, Kirpichnikov, M.P., and Orekhov, P.S. (2021). Effects of Mutations in the Receptor-Binding Domain of SARS-CoV-2 Spike on its Binding Affinity to ACE2 and Neutralizing Antibodies Revealed by Computational Analysis. BioRxiv 2021.03.14.435322.

Casadevall, A., Henderson, J., Joyner, M., and Pirofski, L. (2021). SARS-Cov2 variants and convalescent plasma: reality, fallacies, and opportunities. J. Clin. Invest. *131*.

690 Case, J.B., Bailey, A.L., Kim, A.S., Chen, R.E., and Diamond, M.S. (2020). Growth, detection,

691 quantification, and inactivation of SARS-CoV-2. Virology *548*, 39–48.

692 Cele, S., Gazy, I., Jackson, L., Hwa, S.-H., Tegally, H., Lustig, G., Giandhari, J., Pillay, S.,

693 Wilkinson, E., Naidoo, Y., et al. (2021). Escape of SARS-CoV-2 501Y.V2 from neutralization by

694 convalescent plasma. MedRxiv 2021.01.26.21250224.

695 Challen, R., Brooks-Pollock, E., Read, J.M., Dyson, L., Tsaneva-Atanasova, K., and Danon, L.

696 (2021). Risk of mortality in patients infected with SARS-CoV-2 variant of concern 202012/1:

697 Matched cohort study. BMJ *372*, 1–10.

698 Chen, L., Xiong, J., Bao, L., and Shi, Y. (2020). Convalescent plasma as a potential therapy for

699 COVID-19. Lancet Infect. Dis. *20*, 398–400.

700 Chen, R.E., Zhang, X., Case, J.B., Winkler, E.S., Liu, Y., VanBlargan, L.A., Liu, J., Errico, J.M.,

701 Xie, X., Suryadevara, N., et al. (2021). Resistance of SARS-CoV-2 variants to neutralization by

702 monoclonal and serum-derived polyclonal antibodies. Nat. Med.

703 Chiem, K., Vasquez, D.M., Park, J.G., Platt, R.N., Anderson, T., Walter, M.R., Kobie, J.J., Ye,

704 C., and Martinez-Sobrido, L. (2020). Generation and characterization of recombinant SARS-

705 CoV-2 expressing reporter genes. BioRxiv 1–15.

706 Cox, J.H., Kljavin, N.M., Ramamoorthi, N., Diehl, L., Batten, M., and Ghilardi, N. (2011). IL-27

707 promotes T cell-dependent colitis through multiple mechanisms. J. Exp. Med. *208*, 115–123.

708 Davies, N.G., Davies, N.G., Abbott, S., Barnard, R.C., Jarvis, C.I., Kucharski, A.J., Munday,

709 J.D., Pearson, C.A.B., Russell, T.W., Tully, D.C., et al. (2021). Estimated transmissibility and

710 impact of SARS-CoV-2 lineage B . 1 . 1 . 7 in England. *3055*, 1–16.

711 Elezkurtaj, S., Greuel, S., Ihlow, J., Michaelis, E.G., Bischoff, P., Kunze, C.A., Sinn, B.V.,

712 Gerhold, M., Hauptmann, K., Ingold-Heppner, B., et al. (2021). Causes of death and

713 comorbidities in hospitalized patients with COVID-19. Sci. Rep. *11*, 1–9.

714 Fabbi, M., Carbotti, G., and Ferrini, S. (2017). Dual Roles of IL-27 in Cancer Biology and

715 Immunotherapy. *2017*.

716   Galloway, S.E., Prabasaj, P., MacCannell, D.R., Johansson, M.A., Brooks, J.T., MacNeil, A.,

717   Slayton, R.B., Tong, S., Silk, B.J., Armstrong, G.L., et al. (2021). Emergence of SARS-CoV-2

718   B.1.1.7 Lineage — United States, December 29, 2020–January 12, 2021. *70*, 95–99.

719   Greninger, A.L., Waghmare, A., Adler, A., Qin, X., Crowley, J.L., Englund, J.A., Kuypers, J.M.,

720   Jerome, K.R., and Zerr, D.M. (2017). Rule-out outbreak: 24-hour metagenomic next-generation

721   sequencing for characterizing respiratory virus source for infection prevention. J. Pediatric

722   Infect. Dis. Soc. *6*, 168–172.

723   Grubaugh, N.D., Gangavarapu, K., Quick, J., Matteson, N.L., Jesus, J.G. De, Main, B.J., Tan,

724   A.L., Paul, L.M., Brackney, D.E., Grewal, S., et al. (2019). An amplicon-based sequencing

725   framework for accurately measuring intrahost virus diversity using PrimalSeq and iVar. 1–19.

726   Hassan, A.O., Kafai, N.M., Dmitriev, I.P., Fox, J.M., Smith, B.K., Harvey, I.B., Chen, R.E.,

727   Winkler, E.S., Wessel, A.W., Case, J.B., et al. (2020). A Single-Dose Intranasal ChAd Vaccine

728   Protects Upper and Lower Respiratory Tracts against SARS-CoV-2. Cell *183*, 169-184.e13.

729   Hojyo, S., Uchida, M., Tanaka, K., Hasebe, R., Tanaka, Y., Murakami, M., and Hirano, T.

730   (2020). How COVID-19 induces cytokine storm with high mortality. Inflamm. Regen. *40*.

731   Horspool, A.M., Kieffer, T., Russ, B.P., DeJong, M.A., Wolf, M.A., Karakiozis, J.M., Hickey, B.J.,

732   Fagone, P., Tacker, D.H., Bevere, J.R., et al. (2021). Interplay of Antibody and Cytokine

733   Production Reveals CXCL13 as a Potential Novel Biomarker of Lethal SARS-CoV-2 Infection.

734   MSphere *6*.

735   Iwasaki, Y., Fujio, K., Okamura, T., Yanai, A., Sumitomo, S., Shoda, H., Tamura, T., Yoshida,

736   H., Charnay, P., and Yamamoto, K. (2013). Egr-2 transcription factor is required for Blimp-1-

737   mediated IL-10 production in IL-27-stimulated CD4+ T cells. Eur. J. Immunol. *43*, 1063–1073.

738   Iyer, S.S., and Cheng, G. (2012). Role of interleukin 10 transcriptional regulation in inflammation

739   and autoimmune disease. Crit. Rev. Immunol. *32*, 23–63.

740   Jin, M., Shean, R.C., Makhsous, N., and Greninger, A.L. (2019). LAVA: a streamlined

741   visualization tool for longitudinal analysis of viral alleles. BioRxiv.

742   Jung, J.Y., and Robinson, C.M. (2014). IL-12 and IL-27 regulate the phagolysosomal pathway in

743   mycobacteria- infected human macrophages. Cell Commun. Signal. *12*, 1–14.

744   Kastelein, R.A., Hunter, C.A., and Cua, D.J. (2007). Discovery and biology of IL-23 and IL-27:

745   Related but functionally distinct regulators of inflammation. Annu. Rev. Immunol. *25*, 221–242.

746   Koboldt, D.C., Chen, K., Wylie, T., Larson, D.E., McLellan, M.D., Mardis, E.R., Weinstock, G.M.,

747   Wilson, R.K., and Ding, L. (2009). VarScan: Variant detection in massively parallel sequencing

748   of individual and pooled samples. Bioinformatics *25*, 2283–2285.

749   Koboldt, D.C., Zhang, Q., Larson, D.E., Shen, D., McLellan, M.D., Lin, L., Miller, C.A., Mardis,

750   E.R., Ding, L., and Wilson, R.K. (2012). VarScan 2: Somatic mutation and copy number

751   alteration discovery in cancer by exome sequencing. Genome Res. *22*, 568–576.

752   Korber, B., Fischer, W.M., Gnanakaran, S., Yoon, H., Theiler, J., Abfalterer, W., Hengartner, N.,

753   Giorgi, E.E., Bhattacharya, T., Foley, B., et al. (2020). Tracking Changes in SARS-CoV-2 Spike:

754   Evidence that D614G Increases Infectivity of the COVID-19 Virus. Cell *182*, 812-827.e19.

755   Kumari, P., Rothan, H.A., Natekar, J.P., Stone, S., Pathak, H., Strate, P.G., Arora, K., Brinton,

756   M.A., and Kumar, M. (2020). Neuroinvasion and encephalitis following intranasal inoculation of

757   SARS-CoV-2 in K18-hACE2 mice. BioRxiv.

758   Laffeber, C., de Koning, K., Kanaar, R., and Lebbink, J.H. (2021). Experimental evidence for

759   enhanced receptor binding by rapidly spreading SARS-CoV-2 variants. BioRxiv.

760   Langmead, B., and Salzberg, S.L. (2012). Fast gapped-read alignment with Bowtie 2. *9*, 357–

761   360.

762   Li, H., and Durbin, R. (2009). Fast and accurate short read alignment with Burrows – Wheeler

763   transform. *25*, 1754–1760.

764   Li, H., Handsaker, B., Wysoker, A., Fennell, T., Ruan, J., Homer, N., Marth, G., Abecasis, G.,

765   Durbin, R., Data, G.P., et al. (2009). The Sequence Alignment / Map format and SAMtools. *25*,

766   2078–2079.

767   Liu, R., Americo, J.L., Cotter, C.A., Earl, P.L., Erez, N., Peng, C., and Moss, B. (2021). One or

768   two injections of MVA-vectored vaccine shields hACE2 transgenic mice from SARS-CoV-2

769   upper and lower respiratory tract infection. Proc. Natl. Acad. Sci. U. S. A. *118*, 1–11.

770   Martin, M. Cutadapt removes adapter sequences from high-throughput sequencing reads.

771   EMBnet.Journal *17.1*, 10–12.

772   McCray, P.B., Pewe, L., Wohlford-Lenane, C., Hickey, M., Manzel, L., Shi, L., Netland, J., Jia,

773   H.P., Halabi, C., Sigmund, C.D., et al. (2007). Lethal Infection of K18-hACE2 Mice Infected with

774   Severe Acute Respiratory Syndrome Coronavirus. J. Virol. *81*, 813–821.

775   Mehra, M.R., Desai, S.S., Kuy, S., Henry, T.D., and Patel, A.N. (2020). Cardiovascular Disease,

776   Drug Therapy, and Mortality in Covid-19. N. Engl. J. Med. *382*, e102.

777   Montagutelli, X., Prot, M., Levillayer, L., Salazar, E.B., Jouvion, G., Conquet, L., Donati, F.,

778   Albert, M., Gambaro, F., Behillil, S. van der, et al. (2021). The B.1.351 and P.1 variants extend

779   SARS-CoV-2 host range to mice. BioRxiv 1–16.

780   Moreau, G.B., Burgess, S.L., Sturek, J.M., Donlan, A.N., Petri, W.A., and Mann, B.J. (2020).

781   Evaluation of K18-hACE2 Mice as a Model of SARS-CoV-2 Infection. Am. J. Trop. Med. Hyg.

782   *103*, 1215–1219.

783   Narayanan, K., Huang, C., and Makino, S. (2008). SARS coronavirus accessory proteins. Virus

784   Res. *133*, 113–121.

785   NIH (2021). NIH halts trial of COVID-19 convalescent plasma in emergency department patients

786   with mild symptoms.

787   O'Toole, Á., S., E., Underwood, A., Jackson, B., Hill, V., McCrone, J., Ruis, C., Abu-Dahab, K.,

788   Taylor, B., Yeats, C., et al. Pangolin: lineage assignment in an emerging pandemic as an

789   epidemiological tool.

790   Oladunni, F.S., Park, J.G., Pino, P.A., Gonzalez, O., Akhter, A., Allué-Guardia, A., Olmo-

791   Fontánez, A., Gautam, S., Garcia-Vilanova, A., Ye, C., et al. (2020). Lethality of SARS-CoV-2

792   infection in K18 human angiotensin-converting enzyme 2 transgenic mice. Nat. Commun. *11*.

793   Ozono, S., Zhang, Y., Ode, H., Sano, K., Tan, T.S., Imai, K., Miyoshi, K., Kishigami, S., Ueno,

794   T., Iwatani, Y., et al. (2021). SARS-CoV-2 D614G spike mutation increases entry efficiency with

795   enhanced ACE2-binding affinity. Nat. Commun. *12*.

796   Pandey, K., Acharya, A., Mohan, M., Ng, C.L., Reid, S.P., and Byrareddy, S.N. (2020). Animal

797   models for SARS-CoV-2 research: A comprehensive literature review. Transbound. Emerg. Dis.

798   Pedersen, B.S., and Quinlan, A.R. (2018). Genome analysis Mosdepth : quick coverage

799   calculation for genomes and exomes. *34*, 867–868.

800   Rambaut, A., Loman, N., Pybus, O., Barclay, W., Barrett, J., Carabelli, A., Connor, T., Peacock,

801   T., Robertson, D.L., and Volz, E. (2020). Preliminary genomic characterisation of an emergent

802   SARS-CoV-2 lineage in the UK defined by a novel set of spike mutations.

803   Sarkar, J., and Guha, R. (2020). Infectivity, virulence, pathogenicity, host-pathogen interactions

804   of SARS and SARS-CoV-2 in experimental animals : a systematic review. Vetinary Res.

805   Commun. *44*, 101–110.

806   Seman, B.G., Vance, J.K., Rawson, T.W., Witt, M.R., Huckaby, A.B., Povroznik, J.M., Bradford,

807   S.D., Barbier, M., and Robinson, C.M. (2020). Elevated levels of interleukin-27 in early life

808   compromise protective immunity in a mouse model of gram-negative neonatal sepsis. Infect.

809   Immun. *88*, 1–15.

810   Shah, M., Ahmad, B., Choi, S., and Woo, H.G. (2020). Mutations in the SARS-CoV-2 spike RBD

811   are responsible for stronger ACE2 binding and poor anti-SARS-CoV mAbs cross-neutralization.

812   Comput. Struct. Biotechnol. J. *18*, 3402–3414.

813   Silvas, J., Morales-Vasquez, D., Park, J.-G., Chiem, K., Torrelles, J.B., Platt, R.N., Anderson,

814   T., Ye, C., and Martinez-Sobrido, L. (2021). Contribution of SARS-CoV-2 accessory proteins to

815   viral pathogenicity in K18 hACE2 transgenic mice. BioRxiv 6.

816   Sims, A.C., Baric, R.S., Yount, B., Burkett, S.E., Collins, P.L., and Pickles, R.J. (2005). Severe

817   Acute Respiratory Syndrome Coronavirus Infection of Human Ciliated Airway Epithelia: Role of

818   Ciliated Cells in Viral Spread in the Conducting Airways of the Lungs. J. Virol. *79*, 15511–15524.

819   Sugiyama, N., Nakashima, H., Yoshimura, T., Sadanaga, A., Shimizu, S., Masutani, K., Igawa,

820   T., Akahoshi, M., Miyake, K., Takeda, A., et al. (2008). Amelioration of human lupus-like

821   phenotypes in MRL/lpr mice by overexpression of interleukin 27 receptor α(WSX-1). Ann.

822   Rheum. Dis. *67*, 1461–1467.

823   Takeda, A., Hamano, S., Yamanaka, A., Hanada, T., Ishibashi, T., Mak, T.W., Yoshimura, A.,

824   and Yoshida, H. (2003). Cutting edge: role of IL-27/WSX-1 signaling for induction of T-bet

825   through activation of STAT1 during initial Th1 commitment. J. Immunol. *170*, 4886–4890.

826   Tegally, H., Wilkinson, E., Giovanetti, M., Iranzadeh, A., Fonseca, V., Giandhari, J., Doolabh,

827   D., Pillay, S., San, E.J., Msomi, N., et al. (2020). Emergence and rapid spread of a new severe

828   acute respiratory syndrome-related coronavirus 2 (SARS-CoV-2) lineage with multiple spike

829   mutations in South Africa. MedRxiv 2020.12.21.20248640.

830   Tian, F., Tong, B., Sun, L., Shi, S., Zheng, B., Wang, Z., Dong, X., and Zheng, P. (2021).

831   Mutation N501Y in RBD of Spike Protein Strengthens the Interaction between COVID-19 and its

832   Receptor ACE2. BioRxiv *19*, 2021.02.14.431117.

833   Toyoshima, Y., Nemoto, K., Matsumoto, S., Nakamura, Y., and Kiyotani, K. (2020). SARS-CoV-

834   2 genomic variations associated with mortality rate of. J. Hum. Genet. 1075–1082.

835   Wang, K., Li, M., and Hakonarson, H. (2010). ANNOVAR: Functional annotation of genetic

836   variants from high-throughput sequencing data. Nucleic Acids Res. *38*, 1–7.

837   Wang, P., Nair, M.S., Liu, L., Iketani, S., Luo, Y., Guo, Y., and Wang, M. (2021). Antibody

838   Resistance of SARS-CoV-2 Variants B.1.351 and B.1.1.7. Nature.

839   Wilm, A., Poh, P., Aw, K., Bertrand, D., Hui, G., Yeo, T., Ong, S.H., Wong, C.H., Khor, C.C.,

840   Petric, R., et al. (2012). LoFreq : a sequence-quality aware , ultra-sensitive variant caller for

841   uncovering cell-population heterogeneity from high-throughput sequencing datasets. *40*, 11189–

842   11201.

843   Winkler, E.S., Bailey, A.L., Kafai, N.M., Nair, S., McCune, B.T., Yu, J., Fox, J.M., Chen, R.E.,

844   Earnest, J.T., Keeler, S.P., et al. (2020). SARS-CoV-2 infection of human ACE2-transgenic

845   mice causes severe lung inflammation and impaired function. Nat. Immunol. *21*, 1327–1335.

846   Wu, Z., and McGoogan, J.M. (2020). Characteristics of and Important Lessons from the

847   Coronavirus Disease 2019 (COVID-19) Outbreak in China: Summary of a Report of 72314

848   Cases from the Chinese Center for Disease Control and Prevention. JAMA - J. Am. Med.

849   Assoc. *323*, 1239–1242.

850   Ye, C., Chiem, K., Park, J., Oladunni, F., Anderson, T., Almazan, F., and Martinez-sobrido, L.

851   (2020a). Rescue of SARS-CoV-2 from a Single Bacterial Artificial Chromosome. 1–10.

852   Ye, Q., Wang, B., and Mao, J. (2020b). The pathogenesis and treatment of the 'Cytokine Storm'

853   in COVID-19. J. Infect.

854   Yinda, C.K., Port, J.R., Bushmaker, T., Owusu, I.O., Purushotham, J.N., Avanzato, V.A.,

855   Fischer, R.J., Schulz, J.E., Holbrook, M.G., Hebner, M.J., et al. (2021). K18-hACE2 mice

856   develop respiratory disease resembling severe COVID-19. PLoS Pathog. *17*, 1–21.

857   Zhao, Q., and He, Y. (2020). Challenges of Convalescent Plasma Therapy on COVID-19. J.

858   Clin. Virol. *127*.

859   Zheng, J., Wong, L.Y.R., Li, K., Verma, A.K., Ortiz, M.E., Wohlford-Lenane, C., Leidinger, M.R.,

860   Knudson, C.M., Meyerholz, D.K., McCray, P.B., et al. (2021). COVID-19 treatments and

861   pathogenesis including anosmia in K18-hACE2 mice. Nature *589*, 603–607.

862   Zhou, D., Dejnirattisai, W., Supasa, P., Liu, C., Mentzer, A.J., Ginn, H.M., Zhao, Y., Duyvesteyn,

863   H.M.E., Tuekprakhon, A., Nutalai, R., et al. (2021). Evidence of escape of SARS-CoV-2 variant

864   B.1.351 from natural and vaccine-induced sera. Cell.

865   (2021a). FACT SHEET FOR HEALTH CARE PROVIDERS EMERGENCY USE

866   AUTHORIZATION (EUA) OF REGEN-COVTM (casirivimab with imdevimab). *564*, 1–30.

867   (2021b). FACT SHEET FOR HEALTH CARE PROVIDERS EMERGENCY USE

868   AUTHORIZATION (EUA) OF BAMLANIVIMAB AND ETESEVIMAB. 1–34.

869